

# Observed seasonal and intraseasonal variability of the East India Coastal Current on the continental slope

A MUKHERJEE, D SHANKAR\*, V FERNANDO, P AMOL, S G APARNA, R FERNANDES,  
G S MICHAEL, S T KHALAP, N P SATELKHAR, Y AGARVADEKAR, M G GAONKAR,  
A P TARI, A KANKONKAR and S VERNEKAR

*CSIR–National Institute of Oceanography (CSIR–NIO), Dona Paula, Goa 403 004, India.*

*\*Corresponding author. e-mail: shankar@nio.org*

We present data from three acoustic Doppler current profilers (ADCPs) moored off Cuddalore (12°N), Kakinada (16.5°N), and Gopalpur (19°N) on the continental slope of the western Bay of Bengal and one mooring on the slope of the northern bay (89°E, 19°N; referred to as being located at Paradip). The data were collected during May 2009 to March 2013 and the observations show that the seasonal cycle, which includes the annual cycle, the semi-annual cycle, and a peak around 120 days, dominates the observed variability of the East India Coastal Current (EICC). Spectral analysis suggests that the 120-day peak dominates the seasonal variability at Paradip and is strong at Gopalpur and Kakinada. The annual cycle is coherent along the western boundary of the bay, i.e., the east coast of India, but with significant phase differences between moorings. At the semi-annual and 120-day periods, the alongshore coherence is weaker. Intraseasonal variability is weaker than the seasonal cycle, particularly at Cuddalore and Paradip, and it exhibits seasonality: the strongest intraseasonal variation is during spring (February–April). Peaks around 12 and 20–22 days are also seen at Gopalpur, Kakinada, and Cuddalore. A striking feature of the currents is the upward phase propagation, but there are also instances when phase propagates downward. The much lower vertical phase speed in the top ~100 m at Cuddalore leads to a distinct undercurrent at this location; at other locations, the undercurrent, though it exists often, is not as striking. During spring, however, the EICC tends to flow poleward (eastward) at Cuddalore, Kakinada, and Gopalpur (Paradip) over the top ~300 m, which is the maximum depth to which observations were made. The cross-shore component of the EICC is much weaker than the alongshore component at Cuddalore and, except for a few bursts during spring, at Kakinada and Gopalpur. It is only at Paradip, on the slope of the northern boundary, that significant cross-shore flows are seen during spring and the summer monsoon (June–August) and these flows are seen to be associated with eddy-like circulations in the altimeter data. We use the ADCP data to validate popular current data products like OSCAR (Ocean Surface Currents Analyses Real-time), ECCO2 (Estimating the Circulation and Climate of the Ocean, Phase II), and GODAS (Global Ocean Data Assimilation System). The OSCAR currents at Paradip match the observed currents well, but the correlation is much weaker at the other three locations. Both ECCO2 and GODAS fair poorly, particularly the latter because its variability in this boundary-current regime is extremely weak. Though it performs badly at Paradip, ECCO2 does capture the observed variability on occasions at the other locations.

---

**Keywords.** Western-boundary current; North Indian Ocean; Bay of Bengal; Acoustic Doppler current profiler; seasonal cycle; intraseasonal variability, time series.

## 1. Introduction

The East India Coastal Current (EICC) (McCreary *et al.* 1996; Shankar *et al.* 1996) is the seasonally reversing western-boundary current (WBC) of the Bay of Bengal (BoB or bay hereafter) (figure 1a, b). The EICC's variability was described earlier primarily using data from ship-drift climatologies (KNMI 1952; Cutler and Swallow 1984; Shetye and Shenoi 1988; Rao *et al.* 1991; Mariano *et al.* 1995), hydrography (Murty 1958; Shetye *et al.* 1991b, 1993, 1996; Murty *et al.* 1993; Sanilkumar *et al.* 1997; Rao 2002; Babu *et al.* 2003; Gangopadhyay *et al.* 2013), Lagrangian drifters (Molinari *et al.* 1990; Shenoi *et al.* 1999), and, more recently, using sea-level anomalies estimated from satellite altimetry (Eigenheer and Quadfasel 2000; Shankar *et al.* 2002; Durand *et al.* 2009). An exhaustive bibliography of the earlier literature on the BoB is available in Varkey *et al.* (1996); reviews of the EICC, which is among the boundary currents of the North Indian Ocean (NIO), are available in Shetye and Gouveia (1998), who described its variability, and Schott and McCreary (2001), who discussed its dynamics as well.

The importance of the EICC, the WBC of the bay, stems from its important role in the basin-scale heat budget and, therefore, local climate (Shenoi *et al.* 2002). The EICC is also important for the biogeochemistry of the western bay (Madhupratap *et al.* 2003; Naqvi *et al.* 2006; Dileepkumar 2006), with basic physical processes like upwelling, entrainment, detrainment, and advection (Vinayachandran *et al.* 2005; McCreary *et al.* 2009) and even eddies (Kumar *et al.* 2004, 2007) playing a role in determining the productivity of the region. These links of the EICC to the regional climate and marine living resources imply that it is important to be able to describe its variability and understand what causes the observed variability.

### 1.1 Climatological seasonal cycle

The monthly climatology of ship drifts (Mariano *et al.* 1995) shows that, poleward of 10°N, the EICC flows poleward (upwelling favourable) during February–August; it flows equatorward during October–December, with the direction in January and September changing along the coast (figure 1c). Equatorward of 10°N, the EICC is mostly equatorward over the entire year; this difference in the EICC direction across 10°N was noted by others too (McCreary *et al.* 1993; Shankar *et al.* 1996) and appears to be consistent in the ship-drift datasets (Cutler and Swallow 1984; Rao *et al.* 1991; Mariano *et al.* 1995). The

data from Lagrangian drifters (Shenoi *et al.* 1999) are inconclusive owing to the gaps in data coverage, but a weekly climatology of geostrophic currents estimated from satellite altimetry (figure 1d) suggests that seasonality of the EICC extends equatorward of 10°N as well. The climatological seasonal cycle of the EICC inferred by Durand *et al.* (2009) from the MAP (Margins Altimetry Project) dataset (Birol *et al.* 2006), which provides a superior resolution of the cross-shore structure of the EICC (Durand *et al.* 2008), also suggests a seasonal change in the direction of the EICC south of 10°N, including the east coast of Sri Lanka. A similar change in direction is seen in the north: during the summer monsoon, when the EICC flows poleward along the Indian east coast, its direction is equatorward north of ~18°N (figure 1) (Shetye *et al.* 1991b; Shankar *et al.* 2002; Vinayachandran and Kurian 2007).

The relationship of the EICC to the circulation in the rest of the bay was first established using hydrographic data. On the basis of a hydrographic survey along 13°N, Shcherbinin *et al.* (1979) showed the presence of a WBC between 81°E and 82°E. While the existence of this WBC along the rest of the coast was confirmed using satellite measurements of sea surface temperature (SST) (Legeckis 1987), a comprehensive description of the EICC was made possible through a series of hydrographic surveys (Shetye *et al.* 1991b, 1993, 1996). These data showed that though the EICC off the Indian east coast (i.e., poleward of 10°N) flows poleward during February–August, there is a difference between the pre-monsoon and summer-monsoon poleward flows. During February–May, the only time during the year when the circulation in the basin resembles that of the major ocean basins, the poleward EICC appears in hydrographic data as the WBC of a seasonal, sub-tropical gyre in the bay (Shetye *et al.* 1993). The hydrographic data suggest that though the poleward EICC throughout February–August is accompanied by coastal upwelling, the poleward flow during February–May extends to greater depths than during the summer-monsoon months of June–August, when the poleward EICC is shallow (~70 m deep) (Shetye *et al.* 1991b). The EICC transport over the top 1000 m during the summer monsoon, when the local winds are strong (Shetye *et al.* 1991b), is also much weaker (~1 Sv = 10<sup>6</sup> m<sup>3</sup>s<sup>-1</sup>) than the transport of 5–10 Sv during March–April, when the local winds are much weaker (Shetye *et al.* 1993). A list of the transport estimates available for the EICC is given in table 1 and shows that the transport of the equatorward EICC during October–December (Shetye *et al.* 1996) is comparable to that of the poleward EICC during February–May.

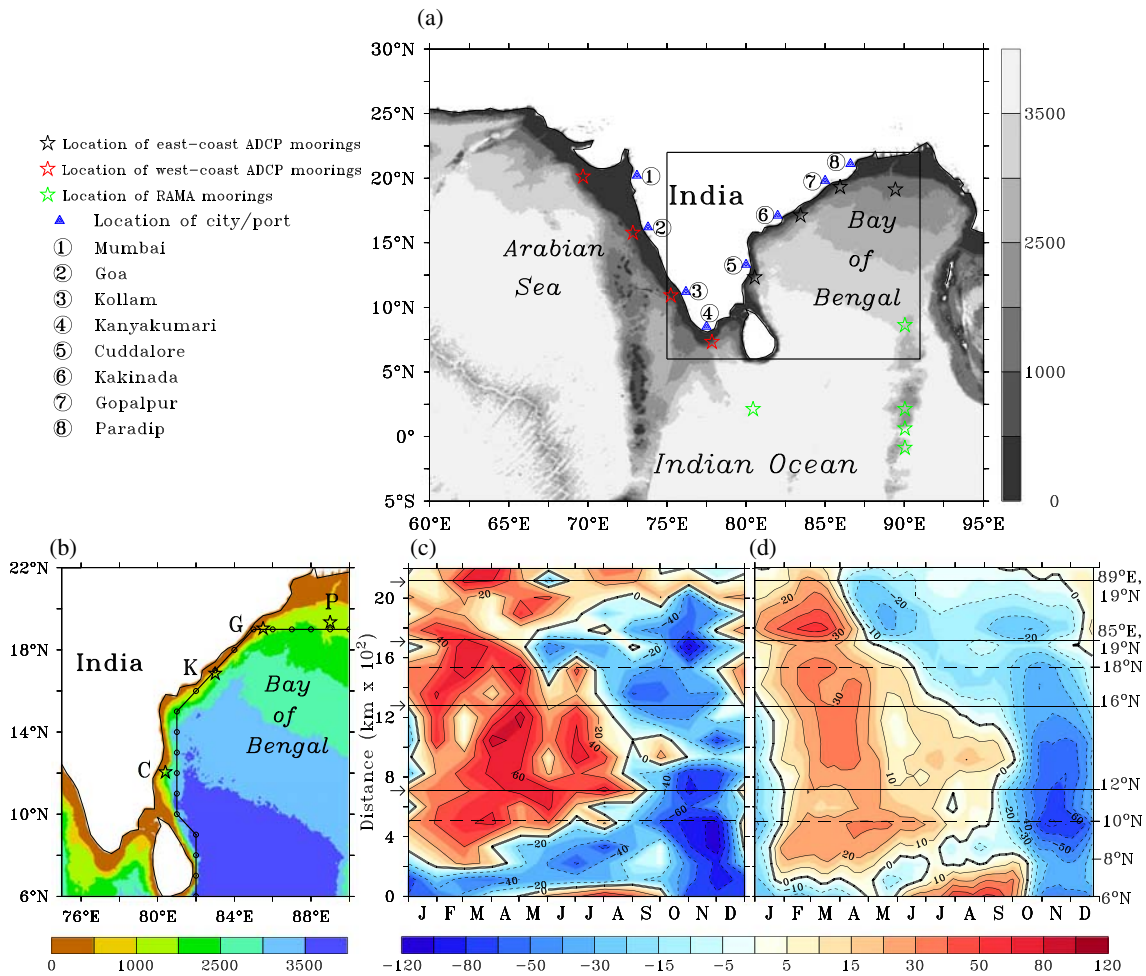


Figure 1. (a) The location of the region of interest in the Indian Ocean; the grey-scale shading shows the bathymetry (m). Moorings along the west coast of India (red stars) were used by Amol *et al.* (2014). The RAMA moorings (green stars) were used by Sikhakolli *et al.* (2013). Moorings along the east coast (black stars) of India are discussed in this manuscript. Names of places mentioned in the text are shown. The box marked by solid lines is the western-bay region shown in panel (b). (b) The western bay, showing the bathymetry (colour scale, m) and the location of all ADCP moorings (black stars). Here, P, G, K, and C (the first letters of the name of the location) denote Paradip, Gopalpur, Kakinada, and Cuddalore, respectively. The small circles and the associated line represent near-coastal locations along which the current climatologies shown in panels (c) and (d) were computed. (c) Monthly climatologies of alongshore ship-drift currents ( $\text{cm s}^{-1}$ ) (Mariano *et al.* 1995) as a function of distance (km) from the southern end at (82°E, 6°N). The solid horizontal lines represent the ADCP locations. 18°N and 10°N are marked by dashed horizontal lines; the former is where the shelf break breaks of the western boundary to mark the edge of the northern-boundary shelf and the latter roughly marks the divide between the two seasonal Ekman-pumping regimes in the basin (McCreary *et al.* 1996). The ordinate axis on the left shows the distance from (82°E, 6°N) in hundreds of km and the latitude is marked on the right ordinate axis. Above the dashed line marking 18°N, the ordinate axis marks the distance computed zonally from (85°E, 19°N) to (89°E, 19°N). In this part of the figure, the alongshore current is the zonal current because the shelf break runs roughly west-east. (d) As in panel (c), but for the weekly climatologies of alongshore geostrophic currents ( $\text{cm s}^{-1}$ ) (AVISO 1996) based on data from January 2000 to December 2008.

These hydrographic data also suggest the presence of an undercurrent (Shetye *et al.* 1991b, 1993, 1996) and recirculations or eddies associated with the EICC (Shetye *et al.* 1991b, 1993, 1996; Sanilkumar *et al.* 1997; Ali *et al.* 1998; Gopalan *et al.* 2000; Babu *et al.* 2003), but the resolution of the hydrographic data in time and space, particularly in the horizontal, make it difficult to interpret the signatures (Shetye *et al.* 1991b, 1993).

### 1.2 Theoretical studies

The Indian subcontinent splits the NIO into two parts, but a connection between the BoB and the Arabian Sea is made possible via the region south of Sri Lanka. Therefore, insight into the dynamics of the NIO depends critically on a coherent description of the circulation off the east and west coasts of India. The hydrographic

Table 1. *Transport estimates of the EICC from hydrographic data.*

| Reference                       | Location | Period (months)                     | Transport estimates in Sv ( $10^6 \text{ m}^3 \text{ s}^{-1}$ )  |
|---------------------------------|----------|-------------------------------------|--|
| Shetye <i>et al.</i> (1991b)    | 10°–20°N | July–August 1989                    | 1 Sv poleward across 13°N  |
| Shetye <i>et al.</i> (1993)     | 10°–20°N | March–April 1991                    | 10 Sv equatorward  |
| Murty <i>et al.</i> (1993)      | 12°N     | April, September, and November 1997 | 3.25 Sv equatorward during April, 3.16 Sv equatorward during September, 6.64 Sv poleward during November |
| Shetye <i>et al.</i> (1996)     | 10°–20°N | December 1991                       | 7.7 Sv equatorward across 13°N   |
| Sanilkumar <i>et al.</i> (1997) | 10°–20°N | 9–23 March 1993                     | 3–17 Sv poleward from 10° to 18°N. At 14°N 3 Sv equatorward  |
| Babu <i>et al.</i> (2003)       | 12°–20°N | 22 March to 28 April 1987           | 12 Sv poleward   |

data collected in the Indian Exclusive Economic Zone (EEZ) during 1987–1994 (Shetye *et al.* 1990, 1991a, b, 1993, 1996) filled a major gap in our description of the EICC and the West India Coastal Current (WICC), permitting theoretical studies that aimed at explaining the observed seasonal cycle. Shetye and Shenoi (1988) and Shetye *et al.* (1993) used the Sverdrup theory (Sverdrup 1947; Stommel 1948) to estimate the EICC transport due to the Ekman-pumping field over the BoB, but a key drawback of this computation was the use of steady-state equations for a circulation whose seasonal cycle is stronger than the mean. Early numerical-modelling studies, which built on similar results from the Pacific (see, for example, Wyrtki 1975; McCreary 1976; Hurlburt *et al.* 1976) and Atlantic (see, for example, O’Brien *et al.* 1978; Picaut 1983; McCreary *et al.* 1984) Oceans, showed that the winds over the Equatorial Indian Ocean (EIO) could have a significant impact on the circulation in the bay, including the EICC, owing to long, baroclinic waves (Potemra *et al.* 1991; Yu *et al.* 1991). A comprehensive study of the dynamics of the Indian Ocean by McCreary *et al.* (1993) showed the importance of remote forcing from the Equator for the seasonal cycle of the EICC. A detailed analysis of the forcing mechanisms of the EICC was carried out by Shankar *et al.* (1996) and McCreary *et al.* (1996), who used a linear, continuously stratified (LCS) model to show that four dynamical processes contributed to the seasonal variation. Apart from the local alongshore winds and Ekman pumping over the BoB, they showed that the winds over the EIO and the winds along the eastern boundary of the BoB (called ‘remote alongshore winds’ by McCreary *et al.* 1996) also contribute to forcing the observed EICC. All four mechanisms were noted to be important, with their relative contributions changing with time (McCreary *et al.* 1996). An analysis using an Ocean General Circulation Model (OGCM) by Vinayachandran *et al.* (1996) led to

similar results. These model simulations show that the reversal in current direction north of  $\sim 18^\circ\text{N}$  during the summer monsoon and off the east coast of Sri Lanka over most of the year is due to the variation in the amplitude of these forcing mechanisms during the year. For example, the equatorial winds, the remote alongshore winds in the eastern bay, and interior Ekman pumping force an equatorward EICC and it is only south of  $\sim 18^\circ\text{N}$  that the poleward EICC forced by the local alongshore winds is able to overcome this equatorward current during the summer monsoon (McCreary *et al.* 1996).

In all these models, the mechanisms for communicating the signal from the source, or forcing, region to remote locations were three long, baroclinic waves: the equatorial Rossby wave, the equatorial Kelvin wave, and the coastal Kelvin wave. The reflection of the equatorial Kelvin wave at the eastern boundary off Sumatra generates an infinity of meridional modes associated with the equatorial Rossby wave (Moore 1968), but only the low-order modes have a real wavenumber and therefore constitute propagating Rossby modes. The high-order modes have an imaginary component in the zonal wavenumber, leading to evanescent waves that decay westward. Moore (1968) showed that these evanescent waves are identical to a  $\beta$ -plane coastal Kelvin wave poleward of the critical latitude, allowing energy to be carried away from the equatorial waveguide. Equatorward of the critical latitude, which occurs poleward of, or close to, the northern boundary of the bay for the first baroclinic mode at the annual and semi-annual periods, the Rossby wave propagates into the interior of the bay, allowing the equatorial winds to influence the seasonal cycle of circulation throughout the bay. The Rossby wave propagates westward across the bay, affecting the EICC (Potemra *et al.* 1991; Yu *et al.* 1991; McCreary *et al.* 1993, 1996; Clarke and Liu 1994; Vinayachandran

*et al.* 1999); similar Rossby waves can be triggered in the BoB by Ekman pumping (or wind curl) as well (Shetye and Shenoi 1988; McCreary *et al.* 1993, 1996; Shetye *et al.* 1993; Shankar *et al.* 1996; Vinayachandran and Yamagata 1998). The winds local to the east coast of India (and Sri Lanka) and the remote alongshore winds trigger coastal Kelvin waves (McCreary *et al.* 1993, 1996; Shankar *et al.* 1996), which propagate with the coast on their right in the northern hemisphere. Furthermore, the huge freshwater inflow into the bay from rivers and rainfall implies a role for freshwater fluxes in forcing the seasonal geostrophic circulation in the western bay (Sprintall and Tomczak 1992; Shetye *et al.* 1993, 1996; Shankar 1998, 2000; Shankar and Shetye 1999, 2001; Han *et al.* 2001b; Han and McCreary 2002; Han and Webster 2002; Vinayachandran *et al.* 2002; Vinayachandran and Kurian 2007; Wu *et al.* 2007).

The distance between the southern tip of Sri Lanka and the Equator ( $\sim 6^\circ$ ) exceeds the sum of the length scales for the gravest vertical (baroclinic) mode for the equatorial wave guide ( $\sim 3^\circ$ ) and the coastal wave guide south of the island ( $\sim 2.5^\circ$ ), permitting the passage of coastal Kelvin waves from the east to the west coast of India (Shankar *et al.* 2002), thereby affecting the WICC and linking the dynamics of the eastern Arabian Sea to that of the BoB and the EIO (McCreary *et al.* 1993; Shankar and Shetye 1997; Bruce *et al.* 1994, 1998; Schott and McCreary 2001; Shankar *et al.* 2002).

### 1.3 Satellite altimetry

The problem of space-time aliasing of the time-dependent circulation of the bay in hydrographic data was ameliorated by satellite altimetry, which provides a quasi-synoptic view of the basin-scale circulation, permitting an analysis of the relationship between the EICC and the circulation in the rest of the bay (Ali *et al.* 1998; Eigenheer and Quadfasel 2000; Gopalan *et al.* 2000; Shankar *et al.* 2002; Gangopadhyay *et al.* 2013). The altimeter data confirm that recirculations and eddies are part of the western-boundary-current system in the bay. The altimeter data also permit an analysis of the EICC variability on time scales longer and shorter than the seasonal cycle.

At interannual time scales, the EICC is influenced by ENSO (El Niño and the Southern Oscillation) and IOD (Indian Ocean Dipole) (Saji *et al.* 1999; Webster *et al.* 1999), the two major climate modes of the Indian Ocean (Clarke and Liu 1994; Rao *et al.* 2002; Han and Webster 2002; Srinivas *et al.* 2005; Jensen 2007; Rao *et al.* 2009; Schott *et al.* 2009; Aparna *et al.* 2012). Using monthly-

mean tide-gauge data, Clarke and Liu (1994) suggested that the interannual EICC would be coherent along the coast, but this inference was shown to be incorrect by Durand *et al.* (2009), who used altimeter data to show that it is decorrelated along the coast. One possible explanation for this alongshore decorrelation at interannual time scales, for which the length scales are expected to be large, was given by Shankar *et al.* (2010), who pointed to the existence of both minima and maxima of interannual variability along the western boundary of the bay. The minima (maxima) occurred along the southern (northern) part of the boundary, implying that the circulation at these time scales would not be correlated in these coastal stretches. This decorrelation can show up as eddies or recirculations, which have also been identified in the altimeter data at interannual time scales (Durand *et al.* 2009; Chen *et al.* 2012).

Durand *et al.* (2009) noted that a similar alongshore decorrelation of the EICC occurred at intraseasonal time scales as well, but this decorrelation was attributed to the existence of eddies along the EICC path and the greater downward bending of the energy expected at these short time scales (Romea and Allen 1983; Nethery and Shankar 2007). Intraseasonal eddies associated with the EICC have received considerable attention in recent times (Durand *et al.* 2009; Kurian *et al.* 2010; Nuncio and Kumar 2012; Cheng *et al.* 2013).

### 1.4 Direct current measurements

A major stumbling block in describing the intraseasonal variability of the EICC is the paucity of direct current measurements, which started only in the 1980s off the Indian east coast. A summary of these observations, which ranged from a day to a few weeks, is provided in table 2. All these observations (Sarma and Rao 1986; Chinthalu *et al.* 2002; Rao 2004; Joseph *et al.* 2006; Sanilkumar *et al.* 2008; Mishra *et al.* 2011) are restricted to short durations and to the near-shore waters, precluding even a description of the seasonal EICC.

Therefore, in order to enable a description of the EICC (and WICC) on time scales ranging from a few hours to years, CSIR–NIO launched an EEZ mooring programme in 2009. Acoustic Doppler current profilers (ADCPs) were deployed on moorings on the shelf and slope off the Indian east coast in 2009. A similar set of moorings were deployed off the west coast as well (Vialard *et al.* 2009; Amol *et al.* 2012, 2014); the longer deployments on the west coast are shown in figure 1(a). Mukherjee *et al.* (2013) used the east-coast ADCP data to describe the near-inertial currents (NICs)

Table 2. List of major direct current measurements along the east coast of India. The estimated maximum velocity is listed in the fourth column.

| Period    | Reference                                     | Location/duration  | Max. velocity/<br>measurement depth         | Remarks  |
|-----------|---|--|---|--|
| 1 day     | Rao (2004)                                    | Central east coast (13°–20°N)  | 37 cm s <sup>-1</sup> /surface<br>(shelf)   | Variation in current along inner shelf off the east coast of India.  |
| < 1 month | Sarma and Rao (1986, 1989)                    | Off river Godavari, 16.5°N/5 days<br>(24–28 September 1980)                | 45.7 cm s <sup>-1</sup> /15 m<br>(shelf)    | Observational evidence of semidiurnal tides, internal waves.         |
|           | Chinthalu et al. (2002); Joseph et al. (2006) | North BoB, 16°N and 19°N/11 days<br>(20–30 September 1997)                 | 60 cm s <sup>-1</sup> /3 m<br>(slope)       | Current structure before and after the 1997 cyclone near Bangladesh. |
| ≥ 1 month | Sanilkumar et al. (2008)                      | Off Yanam, 16.5°N/40 days<br>(August–October 2005)                         | 54.5 cm s <sup>-1</sup> /5 m<br>(shelf)     | Current measurement after passage of cyclone.                        |
|           | Mishra et al. (2011)                          | Gopalpur, 19°N/97 days (May–August 2008)                                   | 74.5 cm s <sup>-1</sup> /surface<br>(shelf) | Impact of currents on beach profiles.                                |
|           | Mukherjee et al. (2013)                       | Along east coast of India, 19°–12°N/3 years<br>(May 2009 to February 2012) | 160 cm s <sup>-1</sup> /40 m<br>(slope)     | Inertial currents on shelf and slope.                                |

on the shelf and slope; they showed that the NICs were stronger on the slope than on the shelf and attributed this result to the east-coast shelf being narrow. The length of the data record allowed them to show seasonal and interannual variability in the generation of the NICs.

### 1.5 Objective

In this paper, we use ADCP data from three moorings on the continental slope off the Indian east coast and one ADCP mooring in deeper waters off the northern boundary of the BoB to quantify the variability of the EICC during 2009–2013. The data used are described in section 2. The alongshore and cross-shore currents are described in sections 3 and 4, respectively. We show that, unlike on the west coast (Amol et al. 2014), the seasonal cycle dominates the variability on the east-coast slope: intraseasonal variability is weaker on the east-coast slope. The data provide evidence for an under-current and upward phase propagation both at seasonal and intraseasonal periods and suggest considerable interannual variability. In order to validate popular current data products, we compare them with the ADCP data in section 5. Section 6 concludes the paper.

## 2. Data

### 2.1 ADCP

We use data from four ADCPs deployed during 2009–2013 (but the length of the data record is not the same for all moorings) on moorings on the continental slope of western and northern BoB. Three moorings, deployed at a water-column depth of ~1100 m off the east coast of India, were located approximately at 19°N (Gopalpur), 16.5°N (Kakinada), and 12°N (Cuddalore) (figure 1b). The fourth mooring was deployed at (89°E, 19°N), i.e., on the slope off the northern BoB; this mooring, which was deployed at a much deeper water-column depth of ~2000 m, is roughly located at the same latitude as Paradip and we therefore use this port as a reference for the mooring. The sampling interval for all ADCPs, which were located at a depth of around 200–300 m, was one hour and the bin size was 8 m. The mooring details are given in table 3. The accuracy of velocity measurements was better than 1.8 cm s<sup>-1</sup>. Following Amol et al. (2012), the gaps in the ADCP data were filled before analysis using the method of Kutsuwada and McPhaden (2002). The currents were then de-tided using the Tidal Analysis Software Kit (TASK) (Bell et al. 1998) software and all tidal constituents with a period of a day or less were

Table 3. Details of ADCP moorings.

| Mooring location | Mooring type | ADCP   | Position       |               | ADCP depth (m) | Water depth (m) | Angle of rotation (°) | Start date | End date |
|------------------|--------------|--------|----------------|---------------|----------------|-----------------|-----------------------|------------|----------|
|                  |              |        | Longitude (°E) | Latitude (°N) |                |                 |                       |            |          |
| Paradip          | Deep         | BNPD1  | 88.997         | 18.998        | 285            | 1695            | 90                    | 23-04-09   | 26-09-10 |
|                  |              | BNPD2  | 88.902         | 19.065        | 350            | 1770            |                       | 16-05-10   | 23-03-11 |
|                  |              | BNBD3  | 88.930         | 19.063        | 325            | 1791            |                       | 23-03-11   | 19-02-12 |
|                  |              | BNBD4  | 88.932         | 19.063        | 296            | 1762            |                       | 19-02-12   | 21-03-13 |
| Gopalpur         | Slope        | BOGD1  | 85.442         | 18.856        | 295            | 1028            | 56                    | 21-04-09   | 15-05-10 |
|                  |              | BOGD2  | 85.796         | 19.381        | 295            | 1027            |                       | 15-05-10   | 21-03-11 |
|                  |              | BOGD3  | 85.786         | 19.380        | 295            | 1040            |                       | 22-03-11   | 17-02-12 |
|                  |              | BOGD4A | 85.787         | 19.380        | 200            | 1053            |                       | 17-02-12   | 10-10-12 |
| Kakinada         | Slope        | BVKD1  | 82.982         | 16.837        | 330            | 1031            | 42                    | 20-04-09   | 13-05-10 |
|                  |              | BOKD1  | 82.497         | 16.387        | 265            | 1003            |                       | 11-05-10   | 27-03-11 |
|                  |              | BOKD2  | 82.521         | 16.4042       | 276            | 1064            |                       | 28-03-11   | 12-02-12 |
|                  |              | BOKD3  | 82.608         | 16.451        | 345            | 1283            |                       | 13-02-12   | 15-03-13 |
| Cuddalore        | Slope        | BOPD1  | 80.203         | 12.015        | 327            | 1087            | 30                    | 26-03-10   | 02-05-11 |
|                  |              | BOPD2  | 80.205         | 12.016        | 320            | 1080            |                       | 03-05-11   | 10-02-12 |
|                  |              | BOPD3  | 80.204         | 12.016        | 325            | 1081            |                       | 10-02-12   | 12-03-13 |

All ADCPs were upward-looking. 75 kHz RDI ADCPs were deployed. The angle of rotation is based on clockwise rotation of the meridional velocity. The original plan was for three ADCP pairs on the slope and shelf of the Indian part of the western boundary (for details of the shelf ADCPs, see Mukherjee *et al.* 2013). Some changes were made in the location owing to logistics (for example, restricted areas) and to facilitate comparison with the HF (high-frequency) radars being deployed by the National Institute of Ocean Technology (NIOT). This need to ensure an overlap with the HF radars led to a shift in the ADCPs at Kakinada (from  $\sim 16.8^\circ$  to  $\sim 16.4^\circ$ N) and Gopalpur (from  $\sim 18.9^\circ$  to  $\sim 19.4^\circ$ N). The ADCP at Paradip ( $89^\circ$ E,  $19^\circ$ N) was added to sample the slope of the northern bay.

removed. The de-tided currents were rotated by minimizing the cross-shore component below 100–150 m using a least-squares approach; above this depth, the cross-shore component was often strong and could not be used to decompose the velocity field. (As in Amol *et al.* (2014), ‘cross-shore’ in this case of slope currents is defined with reference to the shelf break, i.e., the 200 m isobath.)

## 2.2 Data products

Three popular data products have been used as a measure of the circulation in the BoB. We use the ADCP data to validate them in the northern and western bay; a similar validation was carried out by Amol *et al.* (2014) for the eastern Arabian Sea.

### 2.2.1 OSCAR

The first product is OSCAR (Ocean Surface Currents Analyses Real-time) (Bonjean and Lagerloef 2002), an ocean-surface-current data product in which the velocities are derived from satellite measurements. SLA from altimeters, wind speed and direction from scatterometers, and SST are used in this diagnostic model to combine the geostrophic, Ekman-Stommel, and thermal-wind relations, yielding a current-vector field representing the average current over the top 30 m

on a  $0.33^\circ$  grid every five days. OSCAR has been used for several studies in the NIO (Ratnam *et al.* 2009; Chacko *et al.* 2012; Sreenivas *et al.* 2012) and has been validated against buoy measurements from the EIO and central BoB (Sikhakolli *et al.* 2013). We compare OSCAR currents with the ADCP measurements in section 5.1.

### 2.2.2 ECCO2 and GODAS

Unlike OSCAR, which is based on satellite data, the other two popular data products, ECCO2 (Estimating the Circulation and Climate of the Ocean, Phase II) (Stammer *et al.* 2002a, b; Menemenlis *et al.* 2005) and GODAS (Global Ocean Data Assimilation System) (Behringer *et al.* 1998; Behringer and Xue 2004; Behringer 2007), are based on Oceanic General Circulation Models (OGCMs).

In ECCO2, a cubed-sphere-model output interpolated on a  $0.25^\circ$  grid, *in situ* temperature, salinity and mean velocity from surface drifters are assimilated using an adjoint method (Marshall *et al.* 1997). The model has 50 vertical levels and thickness ranges from 10 m near the surface to approximately 450 m at a depth of 4150 m; the output is available every three days. ECCO2 has been used for a large number of oceanographic and interdisciplinary studies, including some in the

NIO (Rao *et al.* 2012; Sreenivas *et al.* 2012) and the EIO (Pandey and Singh 2010). A list of publications and reports since 2005 till date can be found at <http://ecco2.org/manuscripts>.

GODAS (Global Ocean Data Assimilation System) (Behringer *et al.* 1998; Behringer and Xue 2004; Behringer 2007), a real-time ocean analysis developed at the National Centers for Environmental Prediction (NCEP), is based on GFDL's (Geophysical Fluid Dynamics Laboratory) MOMv3 (Modular Ocean Model version 3) (Pacanowski and Griffies 1998) and the data are assimilated in a 3D-VAR scheme (Derber and Rosati 1989). The model has 40 vertical levels with 10 m bins in upper 200 m and the resolution is  $1^\circ \times 1^\circ$  ( $1^\circ \times 0.33^\circ$  near the Equator). GODAS is forced by the momentum, heat, and freshwater fluxes from the NCEP Atmospheric Reanalysis (version) 2. The output is available every five days. The product has been used for a few studies in the NIO (Chacko *et al.* 2012; Rao *et al.* 2012; Wu *et al.* 2012) and a modified version of this product is used in the Indian Ocean Forecast System (INDOFOS) (Ravichandran *et al.* 2013).

We compare ECCO2 and GODAS currents with the ADCP measurements in section 5.2.

### 3. Alongshore currents

The analysis presented in this paper is restricted to the subinertial currents, but we do present spectra for the complete, de-tided current field to permit comparison of the subinertial and inertial components. Since the inertial period at the southernmost location is  $\sim 50$  hrs, a 60-hr low-pass filter (fourth-order Butterworth) was used to retain only the subinertial currents.

#### 3.1 Subinertial currents

We begin with the alongshore, subinertial current, which is strong at Kakinada and Gopalpur and weaker at Cuddalore and Paradip (figure 2). The sign convention used is that the upwelling-favourable current is positive; the positive current is therefore poleward at Cuddalore, Kakinada, and Gopalpur and eastward at Paradip. In the description that follows, we use the terms spring, summer monsoon, and winter to refer to the periods February–April, June–August, and October–December, respectively. This distinction is based on the earlier literature and supported by the ADCP data; January, May, and September represent the transition between these seasons.

In general, these data confirm what was known about the EICC from earlier observations, but the current shows considerable variability within a

season and across years. As inferred earlier from hydrography and ship drifts, the EICC is at its peak strength during spring, when it flows poleward over the top 40–300 m, the depth range sampled in these measurements. The peak value recorded was  $160 \text{ cm s}^{-1}$  at Kakinada during April 2010. The poleward flow weakens during the summer monsoon, particularly below 100 m, and it usually reverses (at 40 m) at Gopalpur and often at Cuddalore as well. During the summer monsoon of 2011, such an equatorward EICC is seen even at Kakinada, suggesting that the EICC during this year was equatorward throughout the east coast over at least part of the summer monsoon. Unlike for the spring EICC, an undercurrent is also seen on occasions during the summer monsoon, but the undercurrent is more prominent during winter, when it generally flows poleward under the equatorward surface current. The undercurrent is more commonly seen at Cuddalore than at the other locations.

A histogram (figure 3a) shows that the alongshore current at Paradip is weaker than  $25 \text{ cm s}^{-1}$  over 80% (90%) of the time at 40 m (100 m). The peak strength at this location is  $100 \text{ cm s}^{-1}$  during the poleward (equatorward) burst in February–March 2010 (April–May 2011). At the other locations, the current is weaker than  $25 \text{ cm s}^{-1}$  just 60% of the time. The histogram is asymmetric with respect to direction, with poleward (eastward) flow dominating at Kakinada (Paradip) and equatorward flow dominating at Gopalpur. It is only at Cuddalore that the distribution tends to be more even. At Kakinada and Cuddalore, the poleward (equatorward) current is stronger than  $25 \text{ cm s}^{-1}$  40% (23%) and 24% (20%) of the time, respectively; in contrast, at Gopalpur, the current is equatorward (poleward) 44% (22%) of the time. This asymmetry implies that the mean current over the record (of over a year) is not as weak as on the west-coast slope (Amol *et al.* 2014). The mean current is poleward at all depths at Kakinada and weakly poleward over the top 150 m at Cuddalore, but it is equatorward up to 180 m at Gopalpur (figure 3b). At Paradip, the mean current reverses at a similar depth and is eastward above it. Therefore, the direction of the mean current at 40 m changes from upwelling-favourable at Paradip to downwelling-favourable at Gopalpur and to upwelling-favourable again at Kakinada and Cuddalore. The standard deviation at the east-coast locations (maximum value is  $29.7 \text{ cm s}^{-1}$ ) is also higher than off the west coast (maximum value  $14.0 \text{ cm s}^{-1}$ ).

A spectral analysis using the Fast Fourier Transform (FFT) shows a strong seasonal cycle at all locations (figure 4); we show both smoothed and unsmoothed spectra for periods greater than



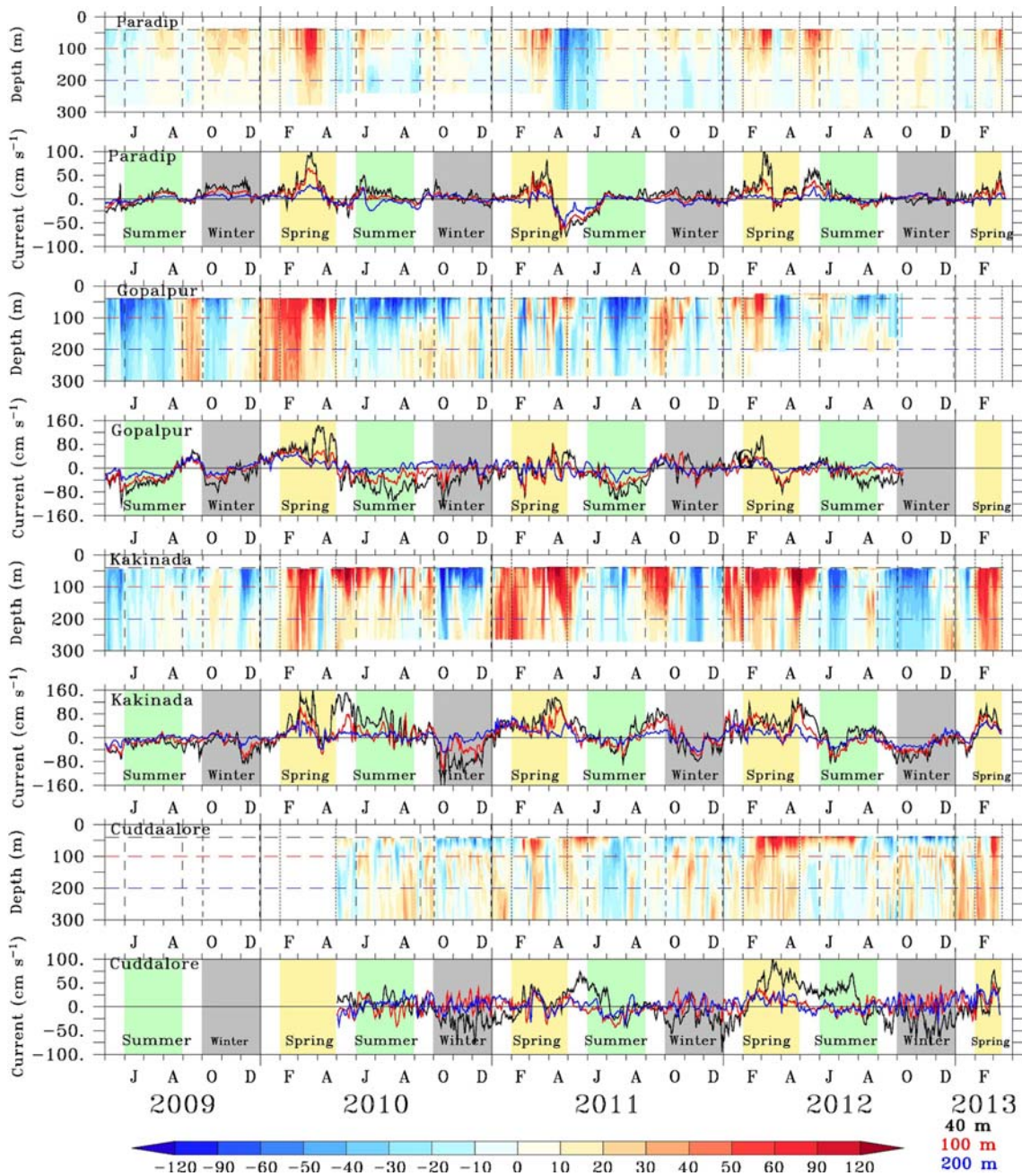


Figure 2. 2.5-day low-pass-filtered, de-tided, residual alongshore currents ( $\text{cm s}^{-1}$ ). At Paradip, the alongshore current is zonal and an eastward current is positive. At the other three locations, a poleward current is positive. This sign convention is used in all figures for the alongshore currents. The solid vertical lines mark the years. The dashed vertical lines in the odd panels and the yellow, green, and gray shading are used to denote the periods spring (February–May), summer monsoon (June–September), and winter (October–December), respectively. The dashed horizontal lines in the odd panels mark the 40 m (black), 100 m (red), and 200 m (blue) depths, and the currents at these depths are plotted in the respective colours in every even panel; the black horizontal line in these panels marks the zero current. The location name is at the top left corner in each panel. Note that the colour scale is not uniform.

100 days because the smoothing, which allows us to determine the confidence interval, averages across the periodicities associated with the seasonal cycle owing to the limited duration of the measurements. In the unsmoothed spectrum, denoted by the red curves, the annual signal is strong on the slope, but is weaker at Paradip. The semi-annual

signal, with a period around 180–200 days, is strong at Gopalpur and Kakinada, but weakens at Cuddalore. The 3–4-monthly peak around 100–130 days is seen at all four locations. It is the strongest component of the seasonal cycle at Paradip and is comparable to the semi-annual cycle at Gopalpur, Kakinada, and Cuddalore. At Cuddalore, this peak

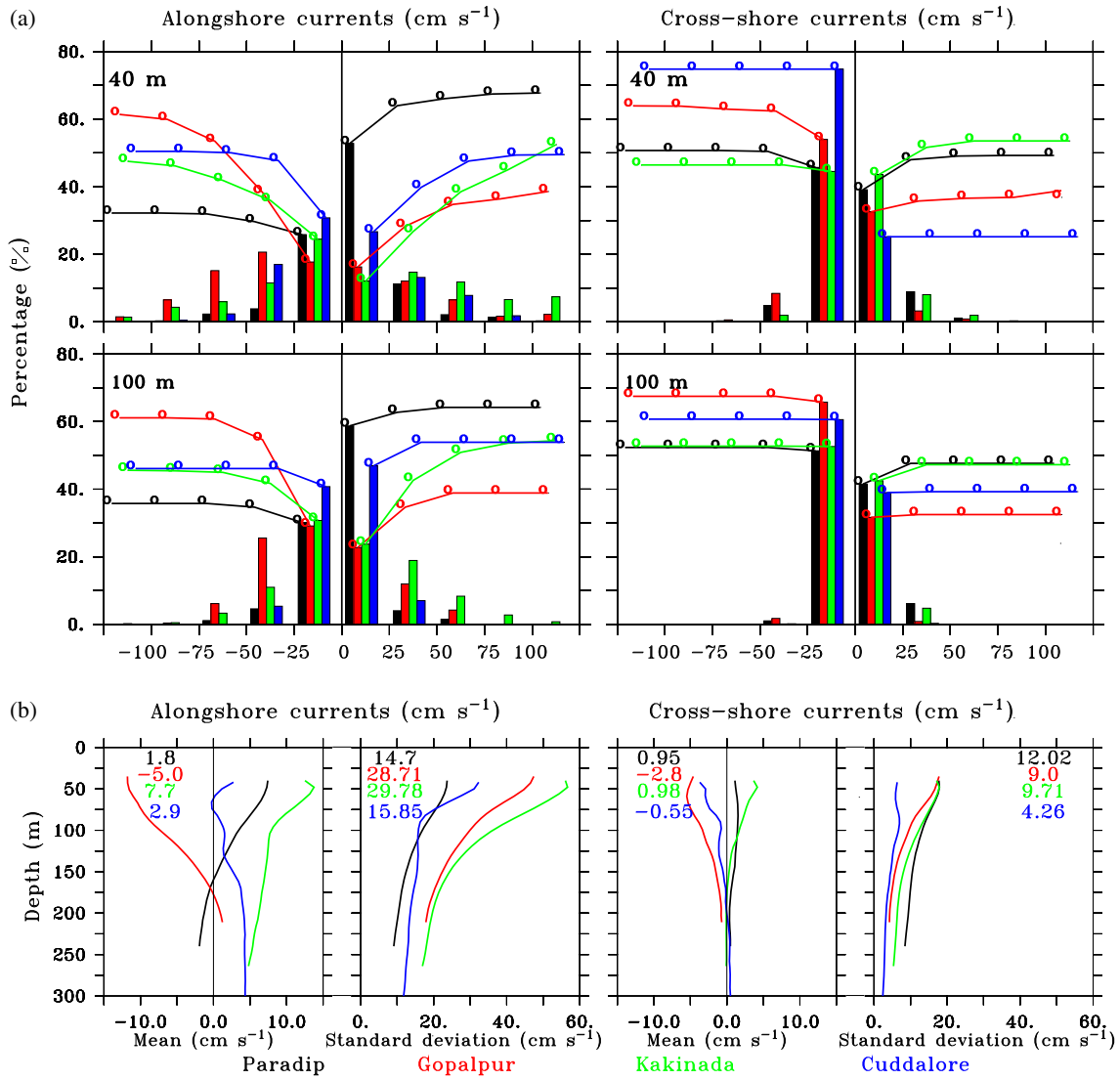


Figure 3. (a) Histogram and cumulative curve for both alongshore (left panels) and cross-shore currents (right panels) at 40 m (top panels) and 100 m (bottom panels) at the four ADCP locations. Here, Paradip, Gopalpur, Kakinada, and Cuddalore locations are represented by black, red, green, and blue colours, respectively. The histogram is calculated over a  $\sim 25 \text{ cm s}^{-1}$  bin (interval) and currents stronger than  $|100| \text{ cm s}^{-1}$  are placed in a single bin. The histogram was computed using data from May 2009 to April 2012 at Paradip, Gopalpur, and Kakinada and from May 2010 to April 2012 at Cuddalore. The cumulative curve, overlaid on the histogram, was drawn separately for negative and positive values of the current. The sum of the occurrences of both positive and negative values adds up to 100% at each location. (b) Statistical mean and standard deviation as a function of depth for both alongshore currents (left panels) and cross-shore currents (right panels). The colours are as in (a). The inset values in the top left corner show the total depth average mean and standard deviation for each location. The period over which the mean and standard deviation were computed is as for the histogram.

occurs at both 100 and 130 days. The peaks in the seasonal part of the spectrum extend to a depth of 100 m (figure not shown); Cuddalore, however, is an exception, and the seasonal peaks decay rapidly with depth at this location.

For periods less than 100 days, i.e., for intraseasonal variability, we look at the smoothed spectrum, which shows strong intraseasonal variability (30–90 days) at 40 m at Kakinada. Comparison of the smoothed spectrum at seasonal and intraseasonal periods shows that the seasonal cycle

is dominant at all locations except Cuddalore, where the difference in the spectral amplitude is within the 95% confidence limit. Peaks occur at 70 days at both Kakinada and Gopalpur, and it is possible that the 60-day peak at Cuddalore is part of this band, which is clearly separated from the peaks at the high-frequency limit of this band (30–40 days). With depth, the intraseasonal peaks tend to decrease fairly rapidly at all locations except Kakinada, where the peaks at 100 m are comparable to those at 40 m (figure not shown).

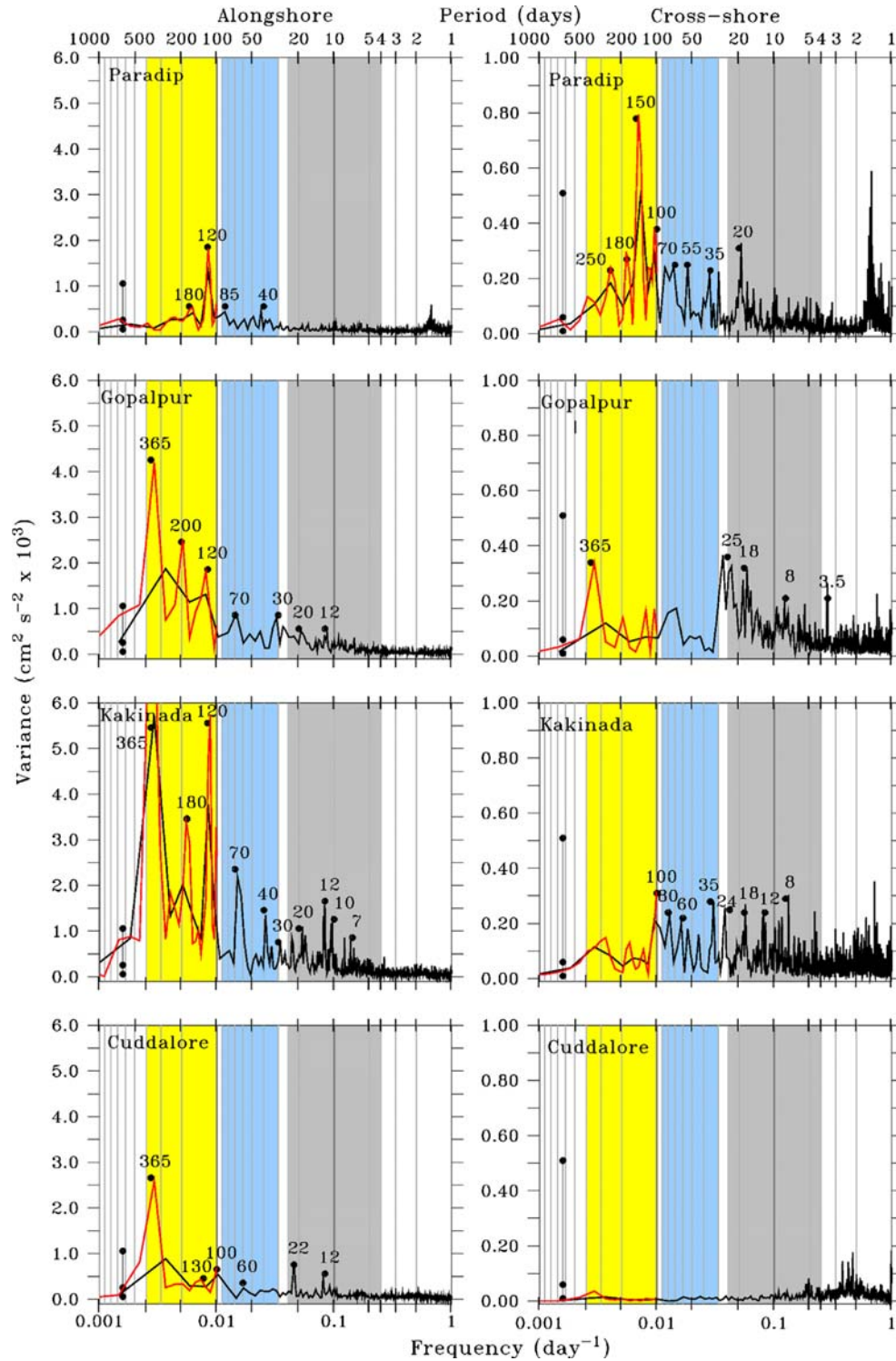


Figure 4. Variance preserving spectra (black curves) for the raw alongshore (left panel) and cross-shore (right panel) currents at 40 m. The spectra were smoothed using a three-point triangle filter after applying a 75% Tukey window to the detrended and detided data. The bar in the lower left corner of all figures represents the 95% confidence interval. The yellow, light blue, and gray shades highlight the seasonal cycle (100–400 days) and the intra-seasonal (30–90 days) and high-frequency (4–25 days) bands, respectively. The dashed red curves show the raw spectra (not smoothed) for the seasonal band. The period for major peaks is listed.

Variability at periods shorter than 30 days is also evident at Kakinada and Gopalpur. One striking peak is at 12 days; this peak, which was also

observed along the west coast of India on both the shelf (Amol *et al.* 2012) and the slope (Amol *et al.* 2014), is seen at all three locations on the east-coast slope.

Since the FFT picks a peak over the entire data record, we use wavelet analysis to document the temporal variability of the spectral power at the seasonal and intraseasonal periods over the 4-year record (figure 5). The wavelet analysis at 40 m shows a strong seasonal cycle and suggests that its amplitude varies over the duration of the record. (Following Amol *et al.* (2014), “we use *suggests* in preference to *shows* because much of the wavelet power at the seasonal periods lies outside the cone of influence (COI), implying that the result does not pass the test of statistical significance. Padding of the data record with zeroes before computing the

wavelet transform also weakens the wavelet power near the end of the data record. This distinction in inference is made throughout this paper, with the use of *suggests* implying a lack of statistical significance, due primarily to the short length of the data record.”) The wavelet analysis suggests that the annual cycle is strong (weak) on the east-coast continental slope (at Paradip) in all years. Higher wavelet power is suggested at periods greater than the annual at Paradip and at Gopalpur and Kakinada. The power for the semi-annual cycle, but not for the peak at 120 days, varies over time. For example, at Kakinada, the analysis suggests

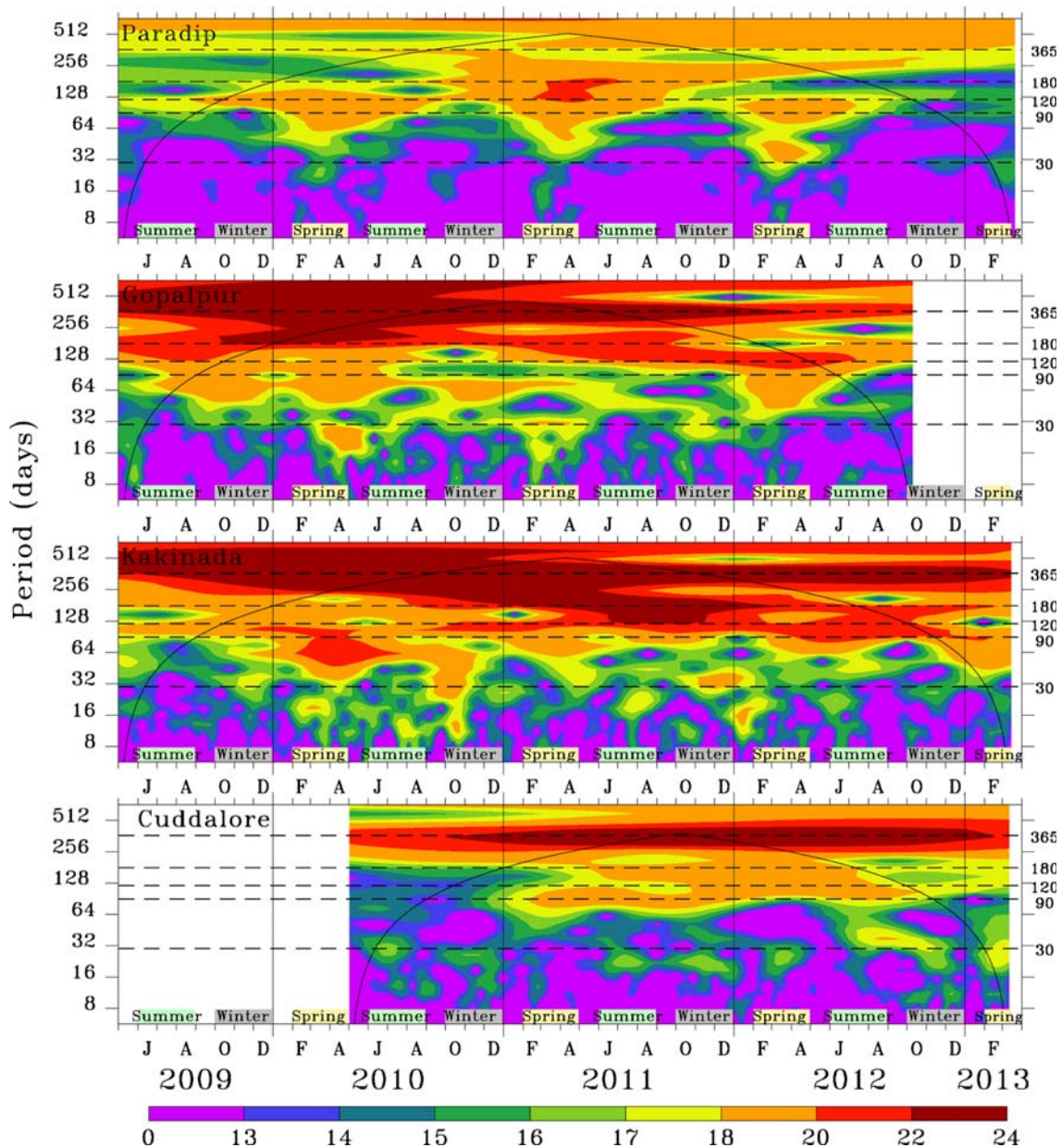


Figure 5. Morlet wavelet power spectra ( $\text{cm}^2 \text{s}^{-2}$ ) of alongshore currents at 40 m depth. The thick black line marks the cone of influence for the wavelet power spectra. The ordinate and wavelet power are plotted on a  $\log_2$  scale. The horizontal dashed lines mark the 30-day, 90-day, 120-day, 180-day, and 365-day periods. Note that the colour scale is not uniform.

that variability at the semi-annual period is greater during 2011 compared to the other years, but this is not so for the 120-day period. We infer that this stronger interannual variability at the semi-annual period suggested by the wavelet analysis leads to the bigger peak at 120 days in the FFT (figure 4; see the red curve depicting the unsmoothed spectrum). Nevertheless, seasonality in the power of the 120-day band is evident at Paradip, Gopalpur, and Kakinada, but not at Cuddalore, where it is seen primarily from July 2011 to June 2012. Similar seasonality is seen in the variability at intraseasonal periods ranging from a few days to 90 days.

Based on the spectral (FFT and wavelet) analysis, we separated the spectrum into a seasonal (period more than 100 days) and an intraseasonal component (periods less than 90 days).

### 3.2 Seasonal cycle

We discuss first the seasonal cycle, which is the variability that can be described by monthly data and is therefore the best documented in the literature (see, for example, Shetye and Gouveia 1998; Schott and McCreary 2001). Included in this seasonal cycle are three bands. The first of these is the annual band, which is forced by the seasonal reversal of the monsoon winds. The second is the semi-annual band, which exists because of the asymmetry in the monsoon winds – this asymmetry is due to the winds being stronger during the summer monsoon compared to the winter monsoon – and forcing from the EIO (McCreary *et al.* 1993, 1996), where a resonance has been noted at the semi-annual period (Jensen 1993; Han *et al.* 1999; Schott and McCreary 2001). The third band is around 120 days and has received much less attention in the literature (Nethery and Shankar 2007; Han *et al.* 2011; Cheng *et al.* 2013; Girishkumar *et al.* 2013).

Unlike on the west-coast slope, where the seasonal cycle was weaker than the intraseasonal variability (Amol *et al.* 2014), the ADCP data show that a strong seasonal cycle exists on the east-coast slope (figures 2 and 4, 5). Low-pass-filtering the currents with a 100-day filter to pick the seasonal variability shows striking differences between the moorings (figure not shown). At Paradip, the current reverses more often in all years and the seasonal component is weaker during winter, when it flows eastward (figure 2). The seasonal current here is eastward during spring as well, and it reaches its peak during this season. During the summer monsoon, the seasonal current at Paradip flows westward in 2011 and 2012 and eastward in 2010. Fewer reversals occur at the locations on the

east-coast slope, with the EICC flowing poleward during spring and equatorward during winter. During the summer monsoon, the seasonal EICC is equatorward at Gopalpur, but can flow in either direction at Kakinada and Cuddalore. To distinguish the annual cycle from the intra-annual components of the seasonal cycle, we use band-pass filters.

Filtering the data with a 300–400-day band-pass filter shows a strong annual cycle on the slope (figure 6). A striking feature of the annual cycle is the upward phase propagation. On occasions, however, as during July–November 2009 at Gopalpur and Kakinada, or during October–December 2012 at Cuddalore, the phase propagates downward. The annual EICC on the slope tends to flow poleward (equatorward) during the first (second) half of the year. The annual cycle decays rapidly with depth at Cuddalore, but a depth–time plot of the wavelet power (figure not shown) suggests that the wavelet power at this period extends to greater depths at Kakinada and, to a lesser extent, at Gopalpur and Paradip.

Band-pass filtering with a 100–250-day filter shows stronger (weaker) currents at Paradip (Cuddalore); at Gopalpur and Kakinada, this intra-annual component of the seasonal cycle is weaker than the annual component, but is still significant (figure 7). At Paradip, there are three full cycles each year, leading to the 120-day peak in the FFT; the intra-annual component is weak, however, following the summer monsoon, leading to the seasonality in the wavelet power spectrum (figure 5). At all locations, the 120-day component strengthens the poleward or eastward EICC (figure 7). If the number of current reversals during a year decreases, as happened at Gopalpur during 2010, the wavelet power tends to be stronger for the semi-annual cycle compared to the 120-day period (figure 5); in 2010, the 100–250-day EICC flowed poleward at Gopalpur during spring and again during winter, with equatorward flow between them during the summer monsoon. The intra-annual current tends to reverse more often when the 120-day peak dominates this part of the seasonal cycle; an example is the stronger 120-day (semi-annual) variability at Kakinada during 2011–2012 (2009–2010). These current reversals in the 100–250-day band tend to occur over the top ~300 m at all locations except Cuddalore, where the wavelet power in this band too tends to be trapped closer to the surface (figure not shown).

Barring the obvious differences in the timing of the reversal, the annual component appears to be coherent along the coast, with the annual EICC flowing poleward or eastward (equatorward or westward) during the first (second) half of the year (figure 6). Following Amol *et al.* (2014), we used Wavelet Coherence Analysis (WCA) to determine

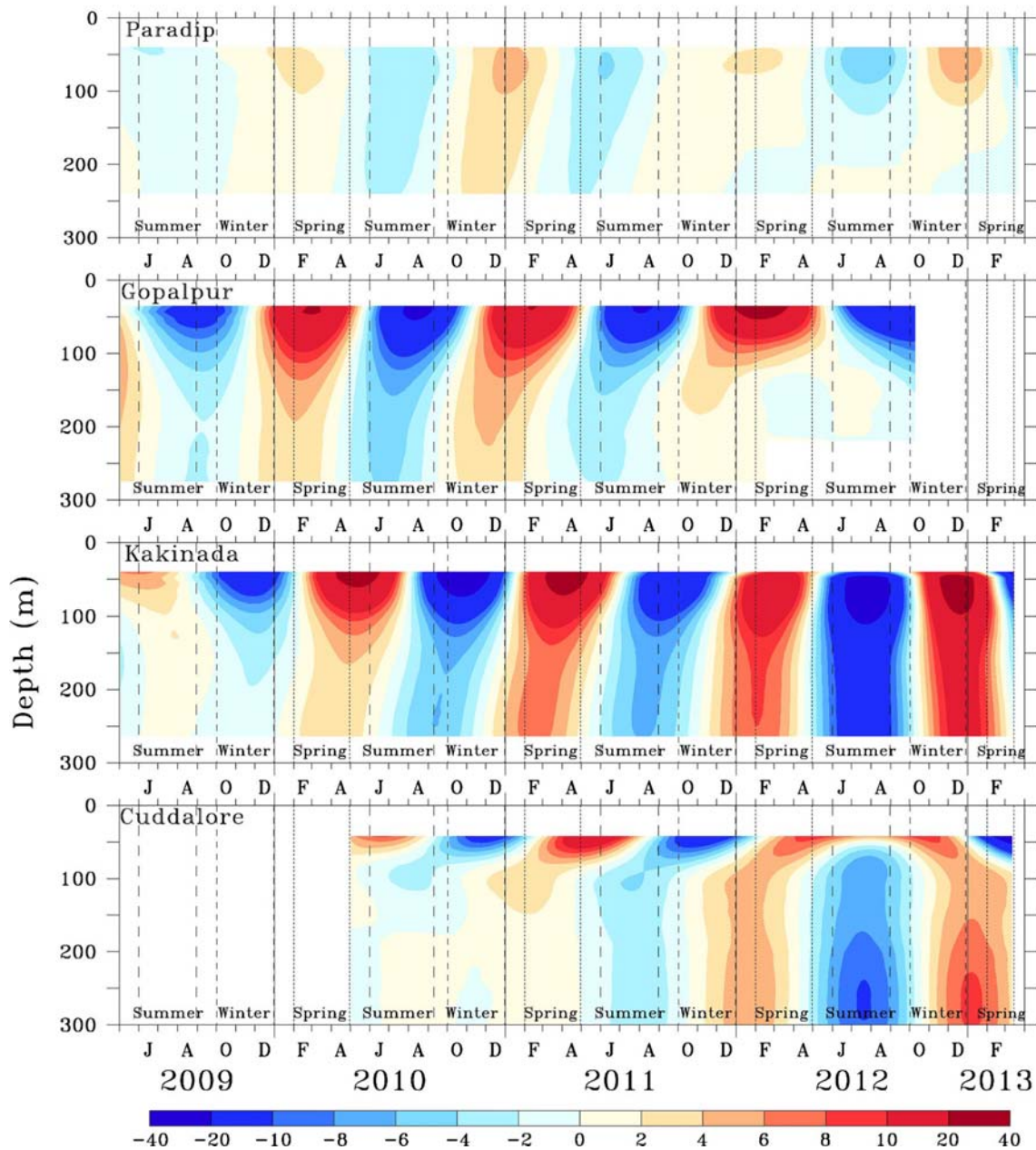


Figure 6. 300–400-day low-pass-filtered alongshore currents ( $\text{cm s}^{-1}$ ). Note that the colour scale is not uniform.

not merely the correlation between the current at adjacent moorings, but also the phase relationship between them. The WCA analysis suggests strong coherence at the annual cycle between successive mooring pairs (figure 8), as was found between the geostrophic EICC across adjacent altimeter tracks by Durand *et al.* (2009). The differences in the timing of the current reversals lead, however, to significant phase differences of up to  $90^\circ$  ( $\sim 90$ – $100$  days). The correlation is maximum between Gopalpur and Kakinada and weaker between Kakinada and Cuddalore; this weakening of the correlation towards the southern part of the coast has been noted earlier (Durand *et al.* 2009). The

coherence is weaker for the intra-annual part of the seasonal cycle.

### 3.3 Intraseasonal variability

Intraseasonal variability is stronger at Kakinada and Gopalpur compared to Paradip and Cuddalore (figure 4). We discuss the observed intraseasonal variability separately for the 30–90-day band, which is the general period range ascribed to the Madden–Julian Oscillation (MJO) (Madden and Julian 1971, 1972, 1993; Han *et al.* 2001a; Vialard *et al.* 2009), and the subinertial periods shorter than 30 days, which we refer to as high-frequency

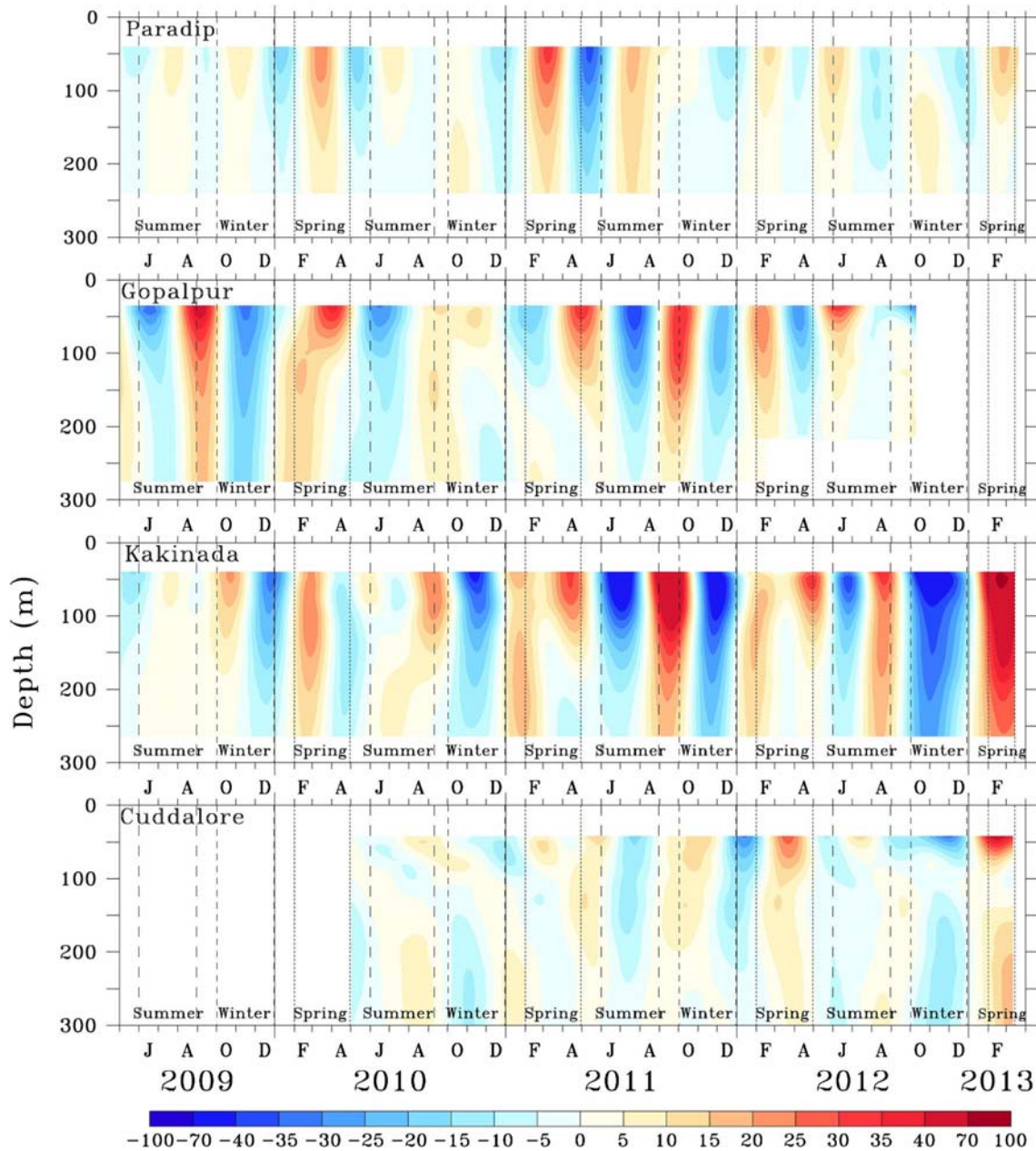


Figure 7. 100–250-day band-pass-filtered alongshore currents ( $\text{cm s}^{-1}$ ). Note that the colour scale is not uniform.

variability. We refrain, however, from ascribing the 30–90-day variability formally to the MJO because it requires a more detailed analysis.

The current in the 30–90-day band is of the order of 40–70 (30–40)  $\text{cm s}^{-1}$  at Gopalpur and Kakinada (Paradip and Cuddalore) (figure 9); these magnitudes are comparable to those of the seasonal component, i.e., 80–90 (55–70)  $\text{cm s}^{-1}$ , at Gopalpur and Kakinada (Paradip and Cuddalore). The variability shows a seasonal pattern, in general, with a peak occurring during spring (figure 9). At locations other than Paradip, variability in this band occurs at other times as well. At Cuddalore,

variability in this band during 2012 is stronger during the summer monsoon than in spring. At Gopalpur and Kakinada, strong variability in this band is seen over most of the year, but there is considerable variation in the pattern from year to year even within this 4-year record. This year-to-year variability was also noted by Durand *et al.* (2009), who, however, pointed to a lack of seasonality in the intraseasonal oscillations. We note here the difference between our definition of intraseasonal variability and theirs: Durand *et al.* (2009) used a 250-day high-pass filter for their intraseasonal variability, thereby including the semi-annual and

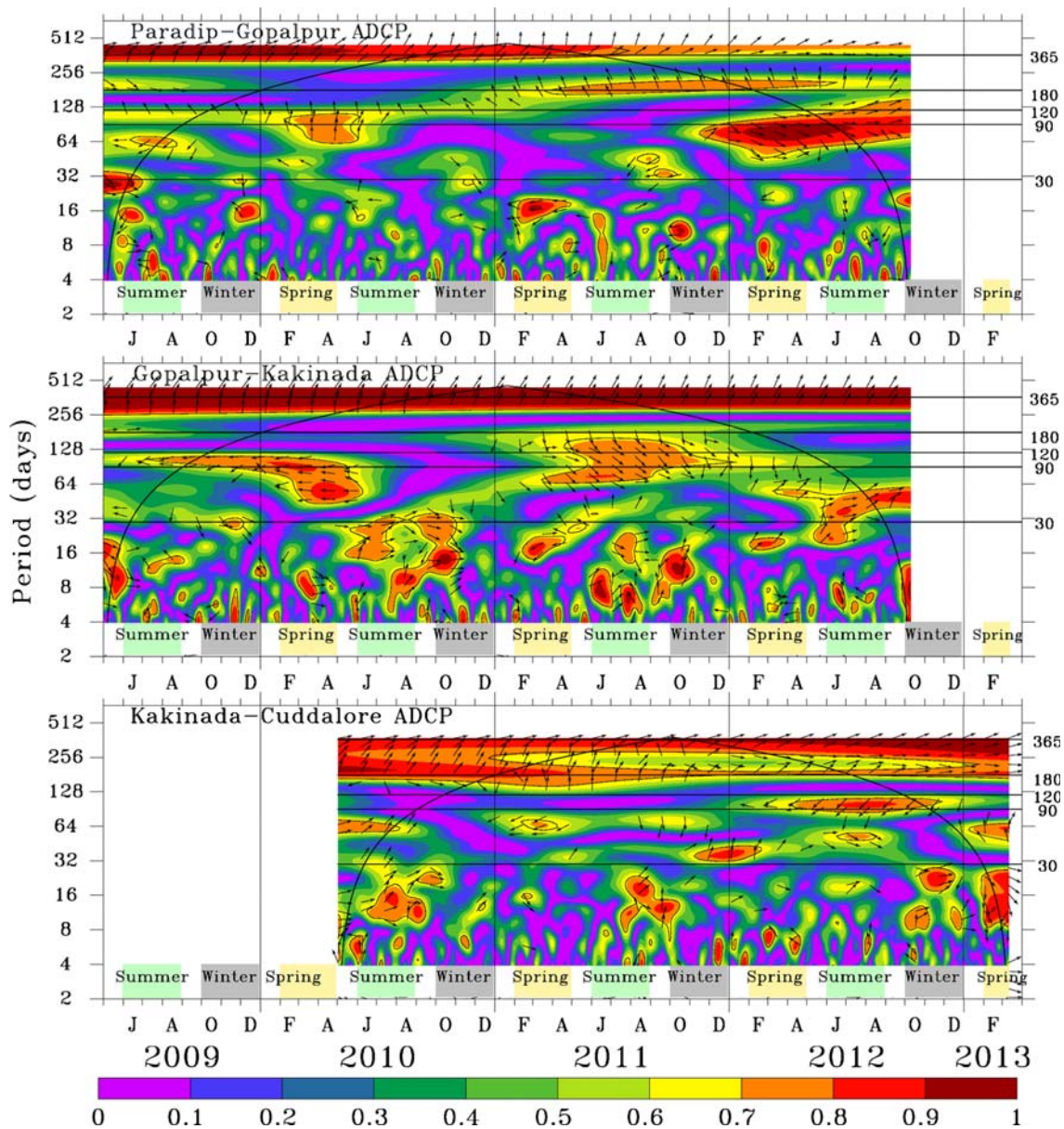


Figure 8. Wavelet coherence for the alongshore currents. The contour line shows the 5% significance level against red noise and the thick black line shows the cone of influence (COI). The arrows show the relative phase relationship with in-phase (anti-phase) pointing right (left). The first station leads (lags) the second station in anticlockwise (clockwise) direction. The arrows are shown only for wavelet coherence of 0.5 or more. In order from top to bottom, the panels show the wavelet coherence for the pairs (a) Paradip–Gopalpur, (b) Gopalpur–Kakinada, and (c) Kakinada–Cuddalore. Note that the ordinate (period) is plotted on a  $\log_2$  scale. The horizontal solid lines mark the 30-day, 90-day, 120-day, 180-day, and 365-day periods.

120-day peaks in this part of the spectrum. Separating the higher periods brings out the difference between the seasonality at Paradip and the relative lack of it at the other locations. Nevertheless, the ADCP data do confirm the alongshore decorrelation at intraseasonal periods (figure 8) noted by Durand *et al.* (2009) in altimeter data. The wavelet coherence is patchy and the phase varies along the coast. As with the annual cycle, variability in this band extends beyond 100 m at Kakinada

and, to a lesser extent, Gopalpur, but tends to be surface-trapped at Paradip and Cuddalore (figure not shown).

A similar variation is seen in the 4–25-day, high-frequency band (figures 10 and 11): high variability at Paradip is restricted to spring, with a weak extension to the summer monsoon. At Kakinada, however, the variability in this band is strong even during winter. As may be expected from the alongshore decorrelation in the 30–90-day band,



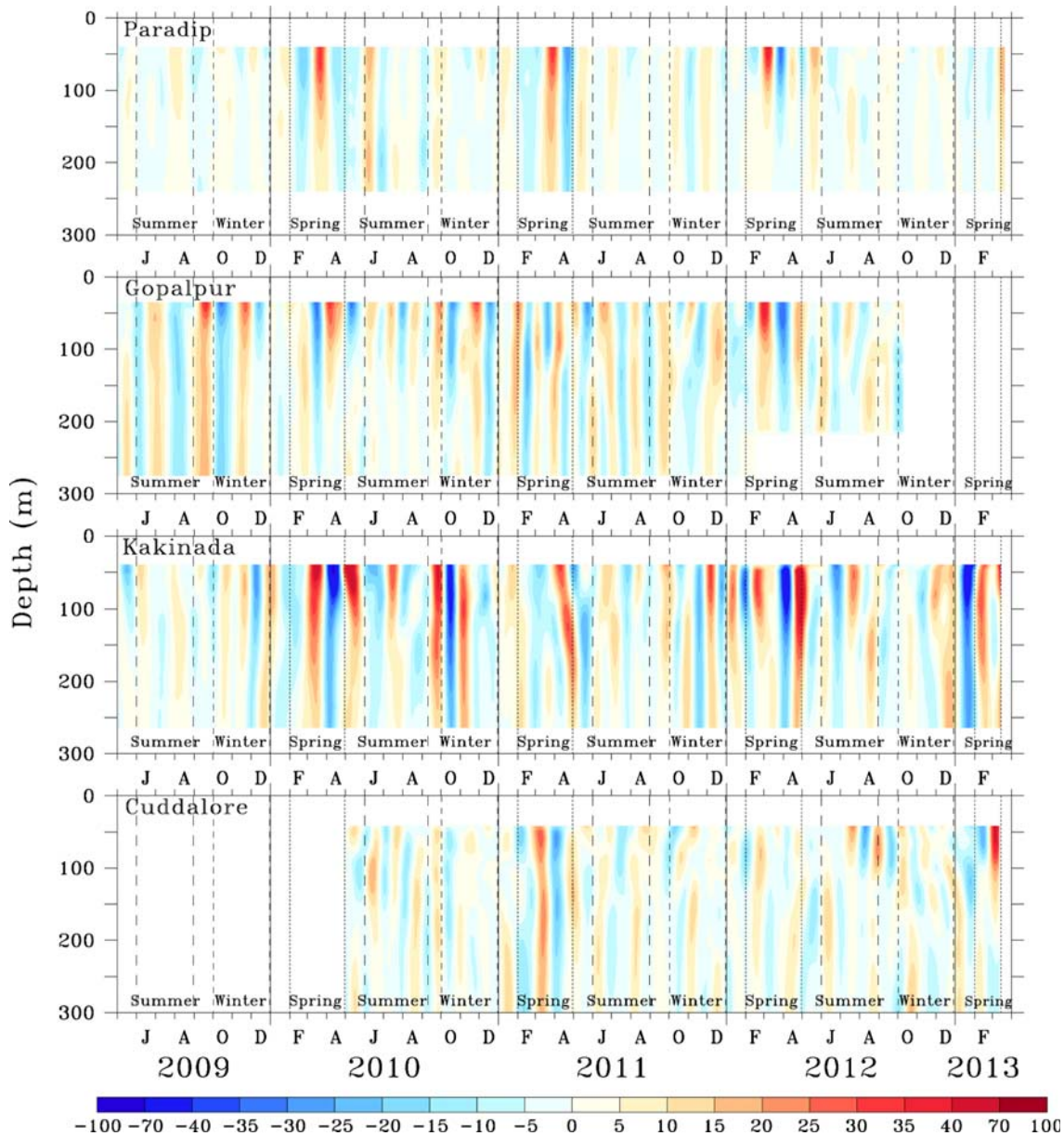


Figure 9. 30–90-day band-pass-filtered alongshore currents ( $\text{cm s}^{-1}$ ). Note that the colour scale is not uniform.

this high-frequency band too decorrelates along the coast (figure 8).

Mukherjee *et al.* (2013) showed that the NIC along the east coast extended to  $\sim 200$  m, much below the shallow mixed layers in the region (Montegut *et al.* 2004; Chatterjee *et al.* 2012). To see if the bursts at the high-frequency end of this 4–25-day band are related to the NICs, we checked the vertically averaged (over 40–200 m) wavelet power for the 1–32-day period range (figure 12). The NICs are clearly separated from the high-frequency band at Paradip, both in time as well as in frequency. A similar separation also exists at Gopalpur, but not at Kakinada and Cuddalore, where the NICs often occur in conjunction with

a burst in the wavelet power at periods ranging from just above the inertial to  $\sim 8$ –12 days. In contrast, allowing for the difference in the colour scale used for the weaker wavelet power in this frequency regime, the wavelet spectrum for periods exceeding 12 days is nearly continuous in time at Cuddalore, Kakinada, and Gopalpur.

### 3.4 Undercurrents

As off the west coast (Amol *et al.* 2014), subsurface energy is not weak off the east coast: there are similar subsurface cores in the wavelet power, particularly at the intraseasonal periods (figure 11).

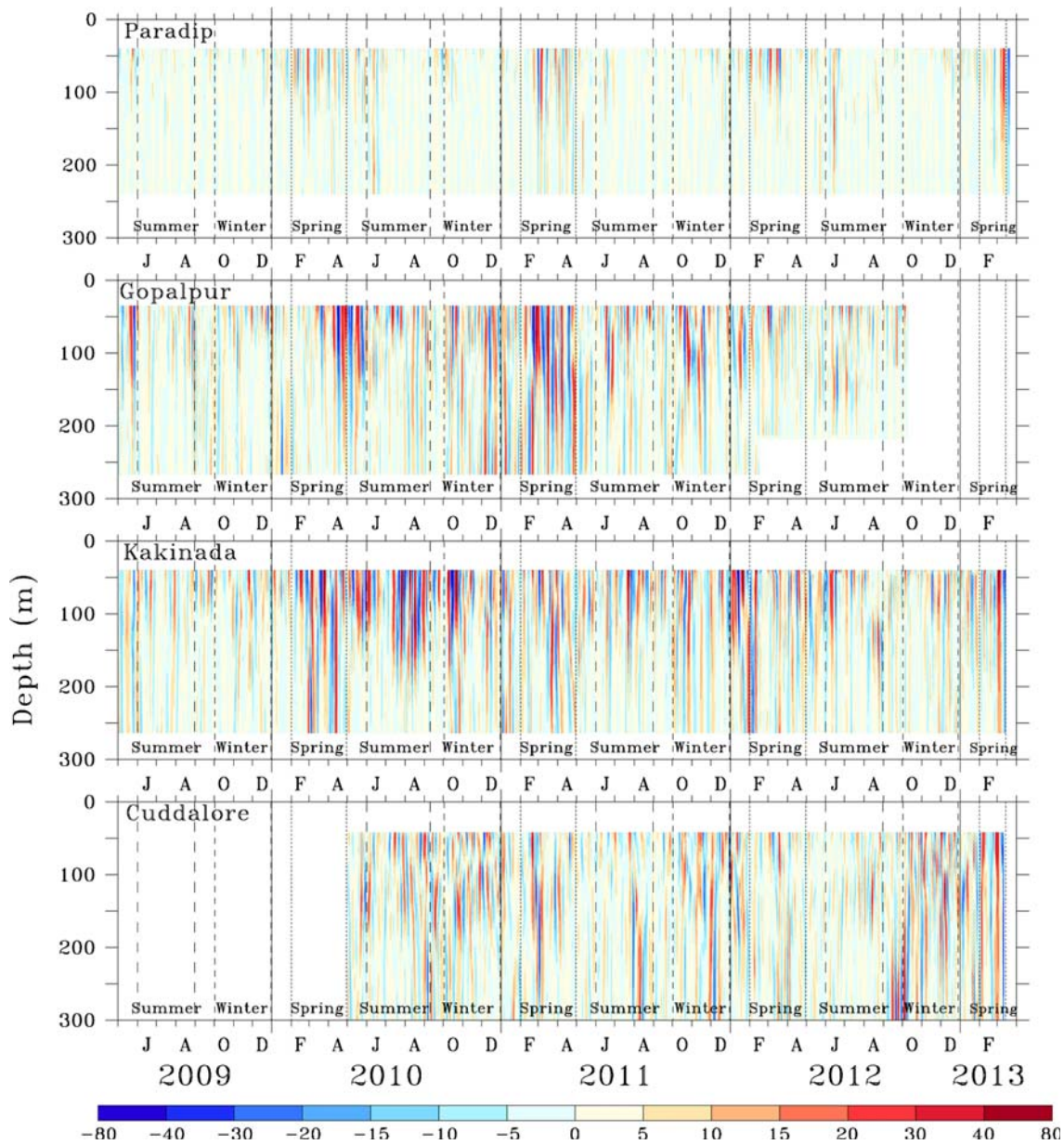


Figure 10. 4–25-day band-pass-filtered alongshore currents ( $\text{cm s}^{-1}$ ). Note that the colour scale is not uniform.

Such subsurface energy maxima suggest the existence of an undercurrent, which was earlier inferred, from hydrographic data, to exist along the Indian east coast (Shetye *et al.* 1991b, 1993, 1996; Rao 2002).

The ADCP data provide evidence for upward phase propagation (figures 6, 7, 9, and 10), but the vertical phase speed for the seasonal cycle is much higher at Paradip ( $\sim 3.8 \text{ m day}^{-1}$ ), Gopalpur ( $\sim 4.1 \text{ m day}^{-1}$ ), and Kakinada ( $\sim 5.5 \text{ m day}^{-1}$ ) compared to the west coast ( $< 1.6 \text{ m day}^{-1}$ ) (Amol *et al.* 2014), leading to a weak undercurrent signature within the top  $\sim 300 \text{ m}$  at these locations. At Cuddalore, however, the vertical phase speed is markedly less in the top  $\sim 100 \text{ m}$  ( $\sim 0.7 \text{ m day}^{-1}$ ), leading to a distinct undercurrent (figure 6).

#### 4. Cross-shore currents

The ADCP data show that the cross-shore current is much weaker than its alongshore counterpart at Cuddalore (figures 2 and 13). (The sign convention is that offshore (upwelling favourable) cross-shore currents are positive: at Paradip, this convention implies that a southward current is positive.) The cross-shore current is weaker than  $25 \text{ cm s}^{-1}$  all the time at Cuddalore and over almost 85% of the data record at the other three locations (figure 3a). The mean flow is weak at all locations, but the standard deviation at Paradip is comparable to that for the alongshore component (figure 3b).

A comparison at 40 m shows that the cross-shore current is weak in comparison to the alongshore

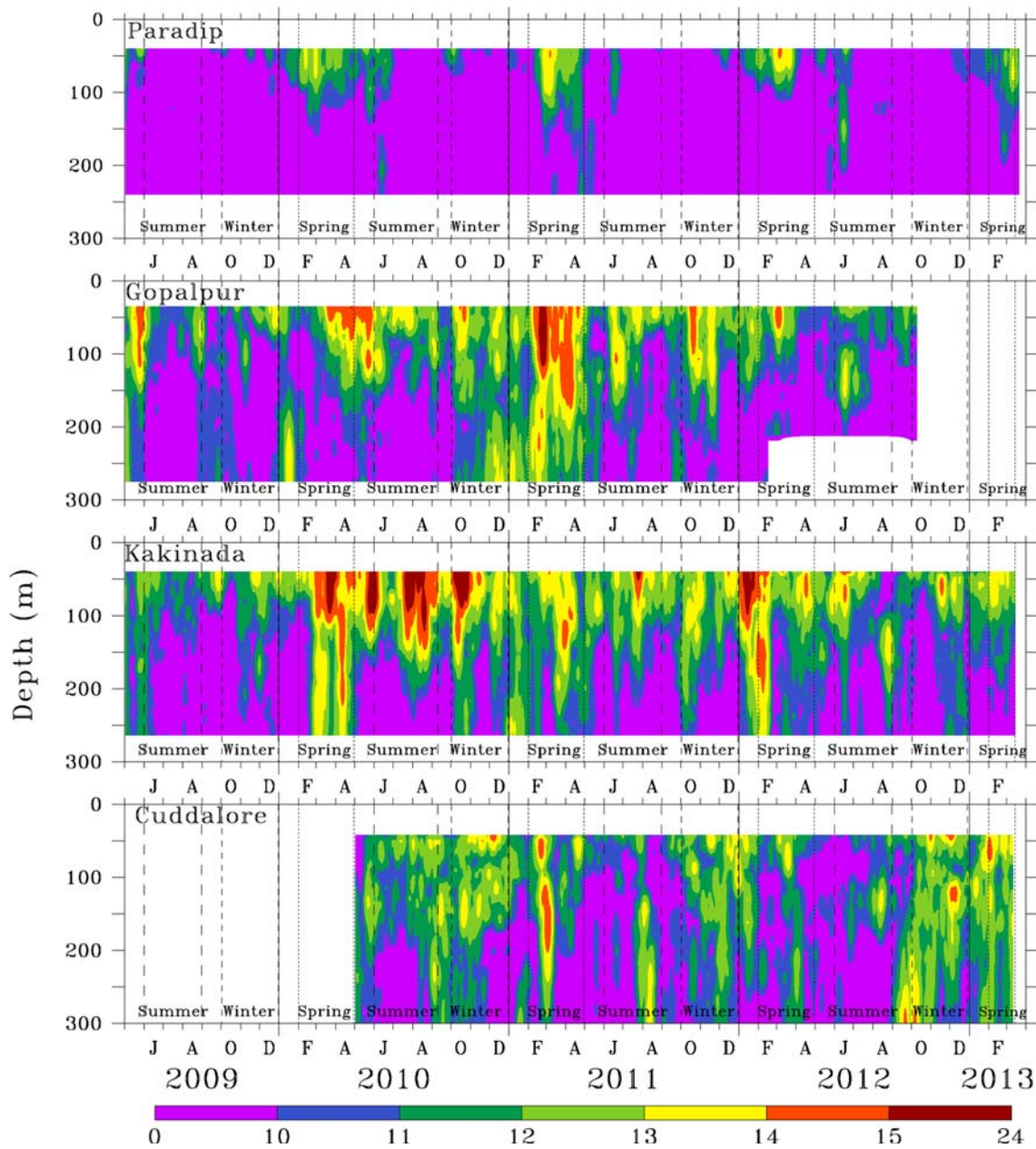


Figure 11. Vertical section of wavelet power ( $\text{cm}^2 \text{s}^{-2}$ ) for 4–25 day band. The ordinate and wavelet power are plotted on a  $\log_2$  scale. Note that the colour scale is not uniform.

component most of the time at Gopalpur and Kakinada (figure 14), but there are a few instances when the cross-shore burst is comparable to the along-shore current at these locations: examples include April 2010 at Gopalpur and April 2011 and 2012 at Kakinada. The nature of variability observed at these two locations leads to several peaks in the FFT (figure 4) and broad peaks, but with little power, in the wavelet spectrum (figure 15). It is only at Paradip, where the cross-shore current peaks during spring (generally offshore) and the summer monsoon (generally onshore) (figure 14), that the FFT and wavelet power tend to show a

higher peak around 100–150 days. We discuss the reasons for this relatively strong cross-shore flow at Paradip in section 6.

The WCA suggests a strong coherence at the annual cycle from Paradip to Kakinada (figure not shown), but it must be noted that the wavelet power at this period is low (figure 15). The bursts during spring (figures 14 and 15) lead to a statistically significant coherence between these two locations, but with a large phase difference. As may be expected for a weak current that shows but a few bursts, the cross-shore component of the EICC decorrelates along the coast.

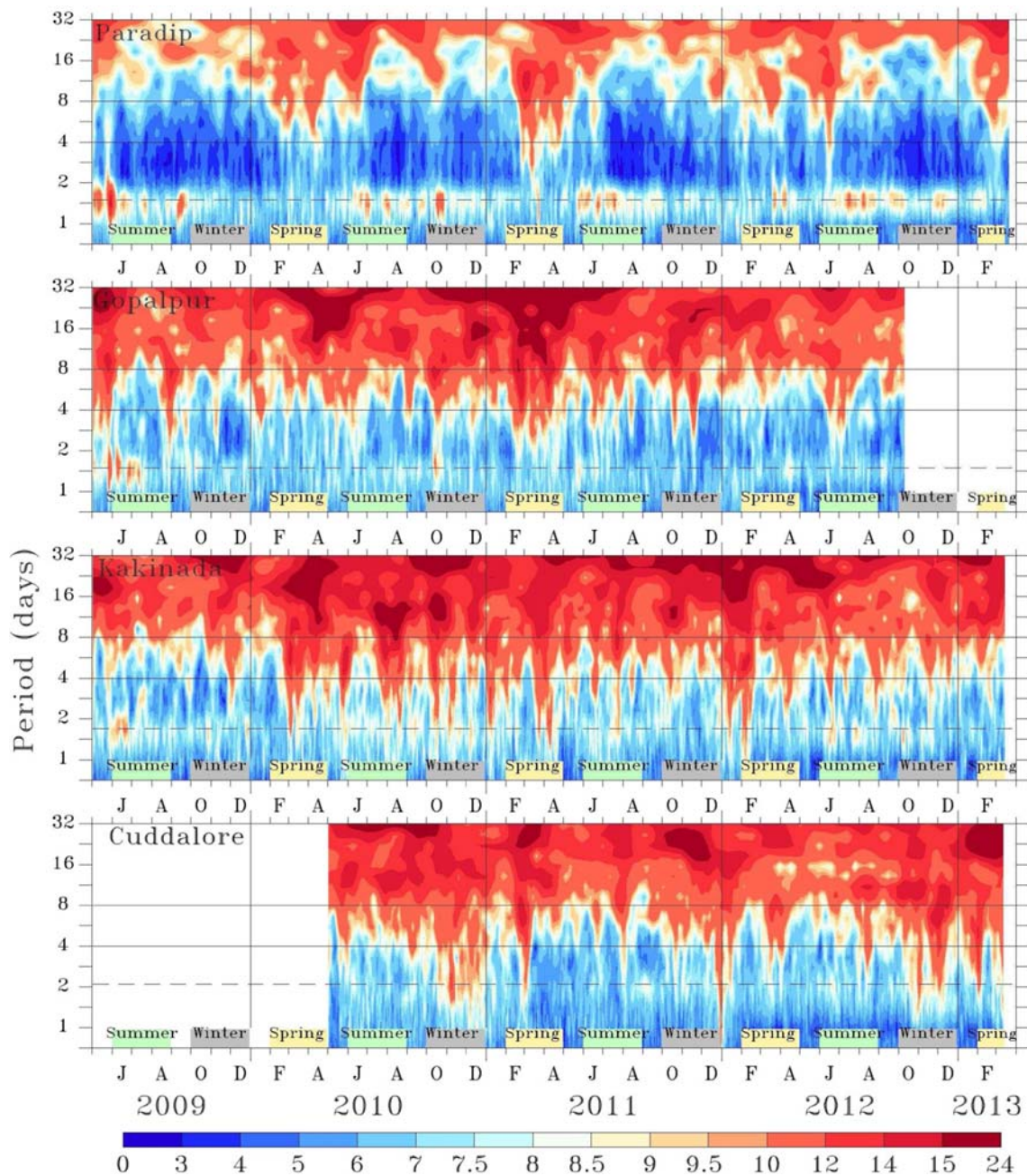


Figure 12. Vertically averaged, over 40–200 m, wavelet power ( $\text{cm}^2 \text{s}^{-2}$ ) for the 1–32-day band. The ordinate and wavelet power are plotted on a  $\log_2$  scale. The 4-day and 8-day periods are highlighted by solid horizontal lines. The dashed horizontal line indicates the theoretical inertial period ( $T = 2\pi/f$ , where  $f = 2\omega \sin \phi$ ;  $\omega$  is the angular frequency of rotation of the earth and  $\phi$  is the latitude) at the location. Note that the colour scale is not uniform.

## 5. Validation of data products

The 4-year-long ADCP data record off the Indian east coast provides an opportunity to validate three current data products – OSCAR, ECCO2, and GODAS – that are widely used in the absence of direct current measurements. For comparison, we pick the grid cell in these products that is nearest the ADCP mooring and use WCA to quantify the goodness of the match. By providing an estimate of not only the correlation at different frequencies,

but also the phases, WCA enables an estimate of the match for each of the major frequency bands discussed above.

### 5.1 OSCAR

Comparison of OSCAR and measured currents has been made earlier (Johnson *et al.* 2007; Sikhakolli *et al.* 2013) and these currents are regularly validated against moored buoys and global drifters

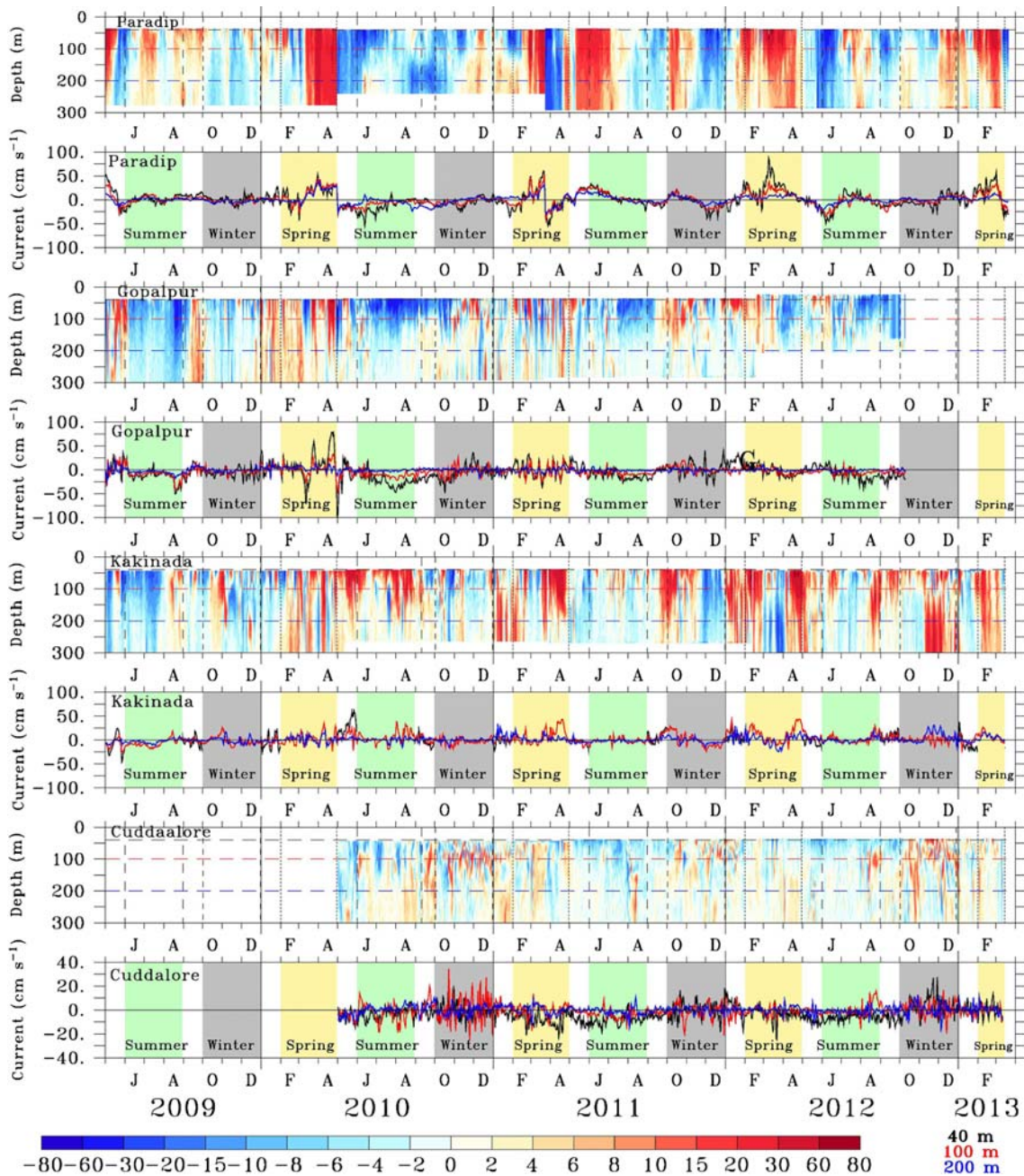


Figure 13. 2.5-day low-pass-filtered, detided, residual cross-shore current ( $\text{cm s}^{-1}$ ). An upwelling favourable current is positive, which implies that the current is positive when it flows offshore (southward at Paradip). The solid vertical lines mark the years. The dashed vertical lines in the even panels and the yellow, green, and gray shading in the odd panels are used to denote the periods spring (February–May), summer monsoon (June–September), and winter (October–December), respectively. The dashed horizontal lines in the odd panels mark the 40 m (black), 100 m (red), and 200 m (blue) depths, and the currents at these depths are plotted in the respective colours in every even panel; the black horizontal line in these panels marks the zero current. The location name is at the top left corner in each panel. Note that the colour scale is not uniform.

(<http://www.oscar.noaa.gov/>). Except within  $10^\circ$  of the Equator, where its reliance on geostrophy implies a poor match with observations, OSCAR has shown fairly good correlation with the *in-situ* current data even though it underestimates the magnitude of the current (Johnson *et al.* 2007). In the EIO and the eastern bay, Sikhakolli *et al.* (2013) showed that the OSCAR zonal current

matched that measured by the RAMA (Research Moored Array for African–Asian–Australian Monsoon Analysis and Prediction) moorings (see figure 1a for the location of these moorings) (McPhaden *et al.* 2009); the match for the meridional component, which showed fluctuations at higher frequencies, was not as good. There are, however, no studies validating OSCAR currents

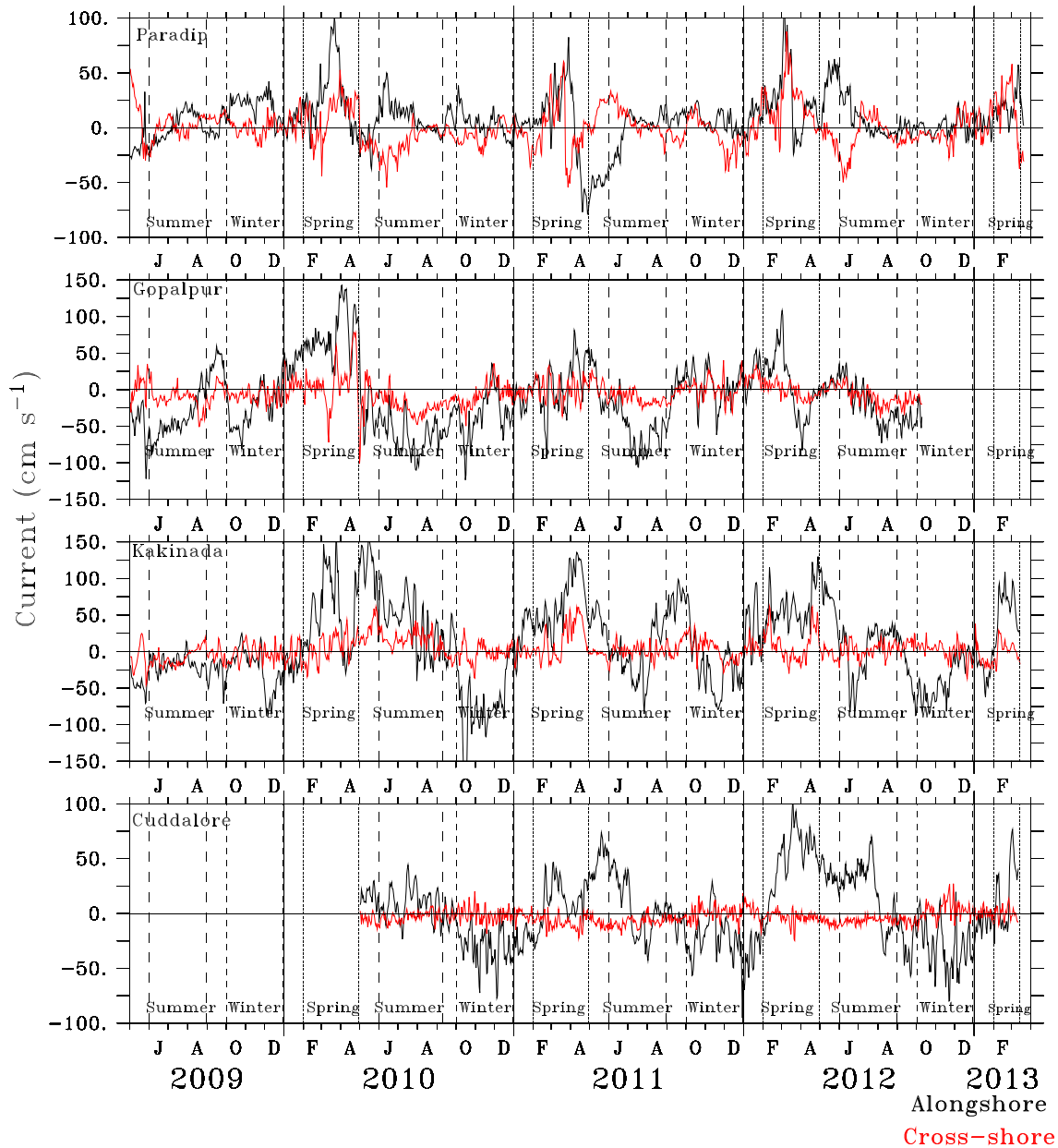


Figure 14. Comparison between alongshore (black) and cross-shore (red) currents ( $\text{cm s}^{-1}$ ) at 40 m depth. The sign convention for the alongshore and cross-shore components is as in figures 2 and 13, respectively.

in the regime of the WBC represented by the EICC. We compare the OSCAR currents, which represent the average current over the top 30 m, to ADCP currents at 40 m depth (the bin closest to the surface). To the best of our knowledge, the only validation of OSCAR against ADCP data for a boundary current was made by Amol *et al.* (2014), who found a high coherence, but with significant phase differences, between ADCP currents off the Indian west coast and OSCAR at seasonal as well as intraseasonal periods; Amol *et al.* (2014) also noted that there were occasions when the OSCAR current was directed opposite to the ADCP current.

The 5-day sampling interval of OSCAR currents implies that they should be able to resolve the seasonal (period greater than 100 days) and intraseasonal (30–90 days) bands, and we do see a reasonable match between OSCAR and ADCP currents (figure 16). The match is particularly good at Paradip (see table 4 for the correlations) owing to the dominance of the seasonal cycle at this location. At other locations, the coherence is high for the annual cycle and in patches for the intra-annual periods, but the match is poor for intraseasonal variability (figure 17), leading to a lower correlation (table 4) than at Paradip. OSCAR is unable to capture the month-long bursts seen in

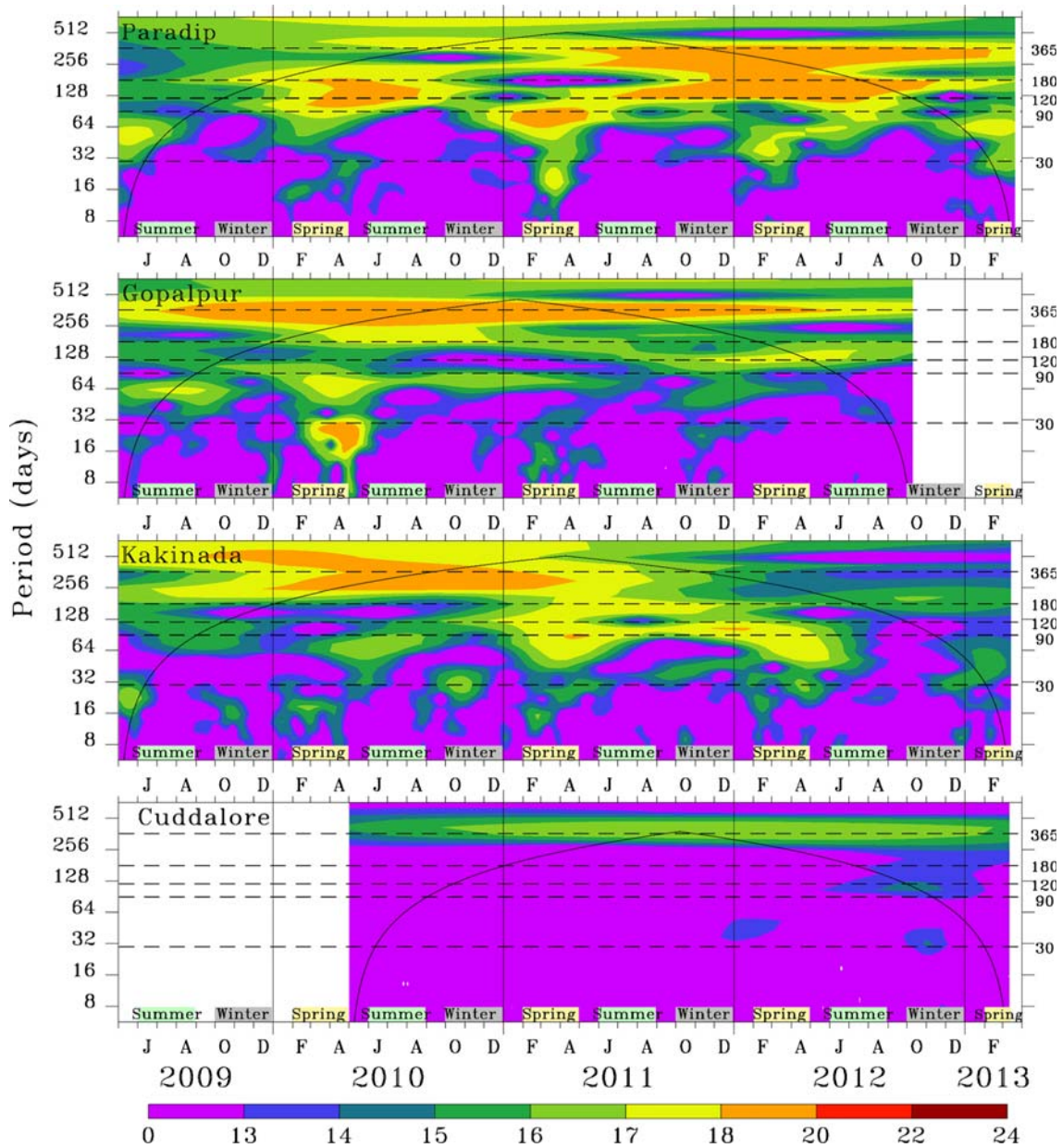


Figure 15. Morlet wavelet power spectra ( $\text{cm}^2\text{s}^{-2}$ ) of the cross-shore currents at 40 m depth. The thick black line shows the cone of influence. The ordinate axis and wavelet power are plotted on a  $\log_2$  scale. The horizontal dashed lines mark the 30-day, 90-day, 120-day, 180-day, and 365-day periods.

the ADCP data at Gopalpur (examples include April 2010 and February and April 2012), Kakinada (examples include February–May 2010 and April 2011), and to a lesser extent, Cuddalore. The correlation is worse for the cross-shore component (table 4).

### 5.2 ECCO2 and GODAS

Unlike with OSCAR, the comparison between the currents at 40 m from the ADCP and ECCO2 is poor at Paradip (figure 16). The match is poor at Kakinada and Cuddalore as well, but is better

at Gopalpur because the annual cycle is simulated well at this location (figure 18). The coherence exceeds 0.8 for the annual cycle at Kakinada and Cuddalore, leading to a correlation of 0.64 for the latter (table 4), but there is a significant difference in phase between the ADCP and ECCO2 currents at Kakinada, leading to a low correlation (table 4). This mismatch is seen even if we use the ECCO2 currents at 5 m or 55 m instead of 40 m. Furthermore, the correlations decrease with increasing depth (figure 19a).

As on the west-coast slope (Amol *et al.* 2014), GODAS simulates much weaker currents on the east-coast slope than is observed (figure 16).

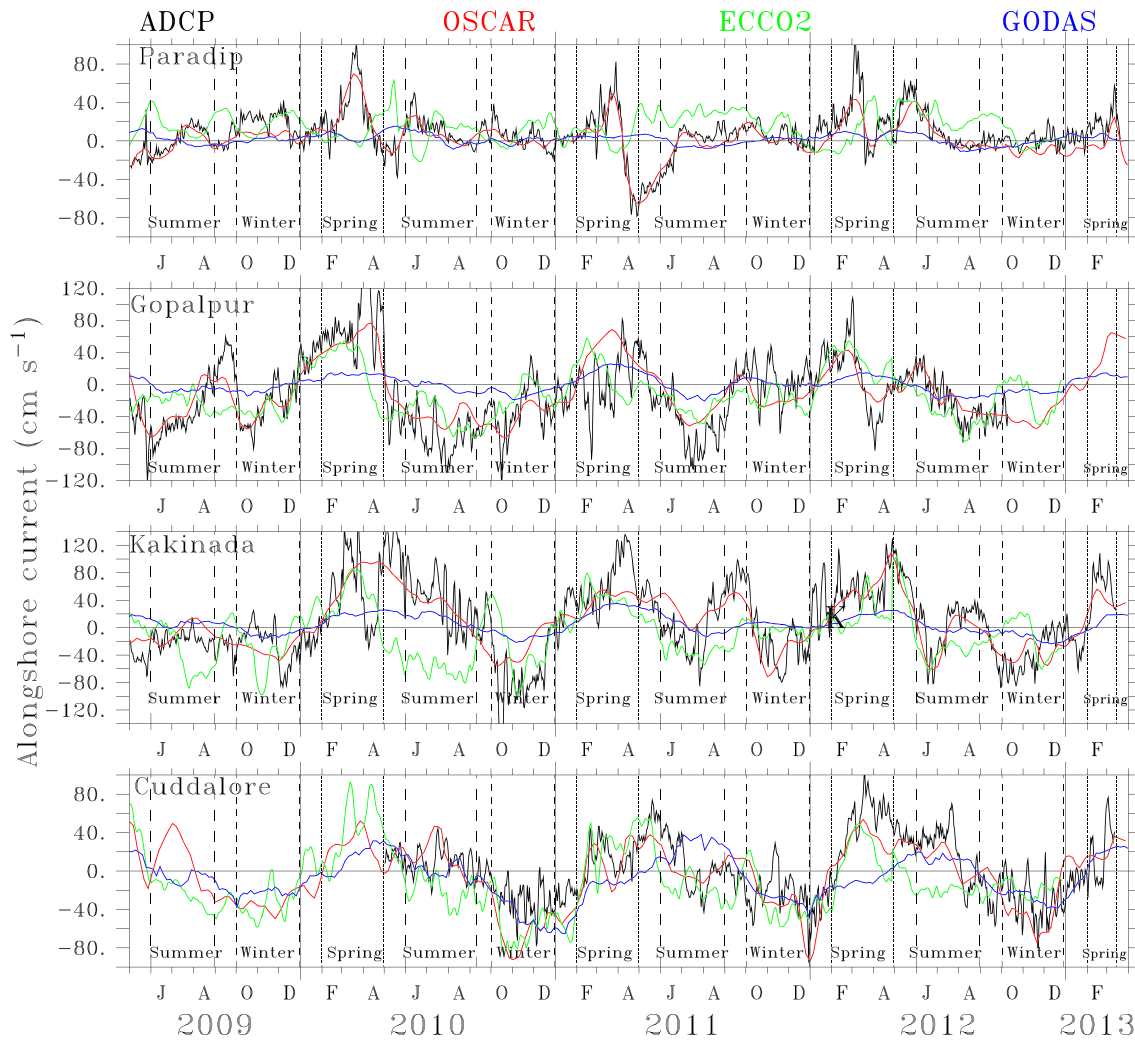


Figure 16. Comparison between alongshore currents ( $\text{cm s}^{-1}$ ) measured by the ADCPs at 40 m and the alongshore currents from OSCAR, ECCO2, and GODAS. The ECCO2 and GODAS currents were picked at the same depth as the ADCP current, i.e., 40 m, but the OSCAR current represents an average over 0–30 m.

Table 4. Correlation between currents from ADCP measurements and data products for both alongshore and cross-shore components of the current.

| Data type | Alongshore   |             |             |             | Crossshore  |             |             |             |
|-----------|--------------|-------------|-------------|-------------|-------------|-------------|-------------|-------------|
|           | P            | G           | K           | C           | P           | G           | K           | C           |
| OSCAR     | <b>0.89</b>  | <b>0.77</b> | <b>0.75</b> | <b>0.71</b> | <b>0.44</b> | <b>0.39</b> | <b>0.47</b> | <b>0.30</b> |
| ECCO2     | <b>-0.36</b> | <b>0.53</b> | <b>0.28</b> | <b>0.64</b> | 0.07        | <b>0.10</b> | -0.02       | <b>0.50</b> |
| GODAS     | -0.03        | <b>0.56</b> | <b>0.64</b> | <b>0.44</b> | <b>0.28</b> | <b>0.10</b> | <b>0.37</b> | <b>0.41</b> |

P, G, K, and C represent Paradip, Gopalpur, Kakinada, and Cuddalore mooring, respectively. Note that alongshore and cross-shore current at Paradip indicates zonal and meridional current, respectively. Correlation values in boldface notation exceed the 99% significance level; the significance of the correlations was computed by comparing the correlations for the filtered time series with the correlations obtained on applying the same Butterworth filter to random time series (Shankar 1998).

Therefore, though the low-frequency variability is simulated well, leading to a fairly high correlation (table 4) and coherence for the annual cycle (figure not shown), the match between the GODAS and observed currents is much worse than for ECCO2. Indeed, the inability of GODAS to

simulate the change in current direction below 100 m at Cuddalore leads to a negative correlation at these depths (figure 19b).

As may be expected, the correlation is worse for the cross-shore component for both ECCO2 and GODAS (table 4).



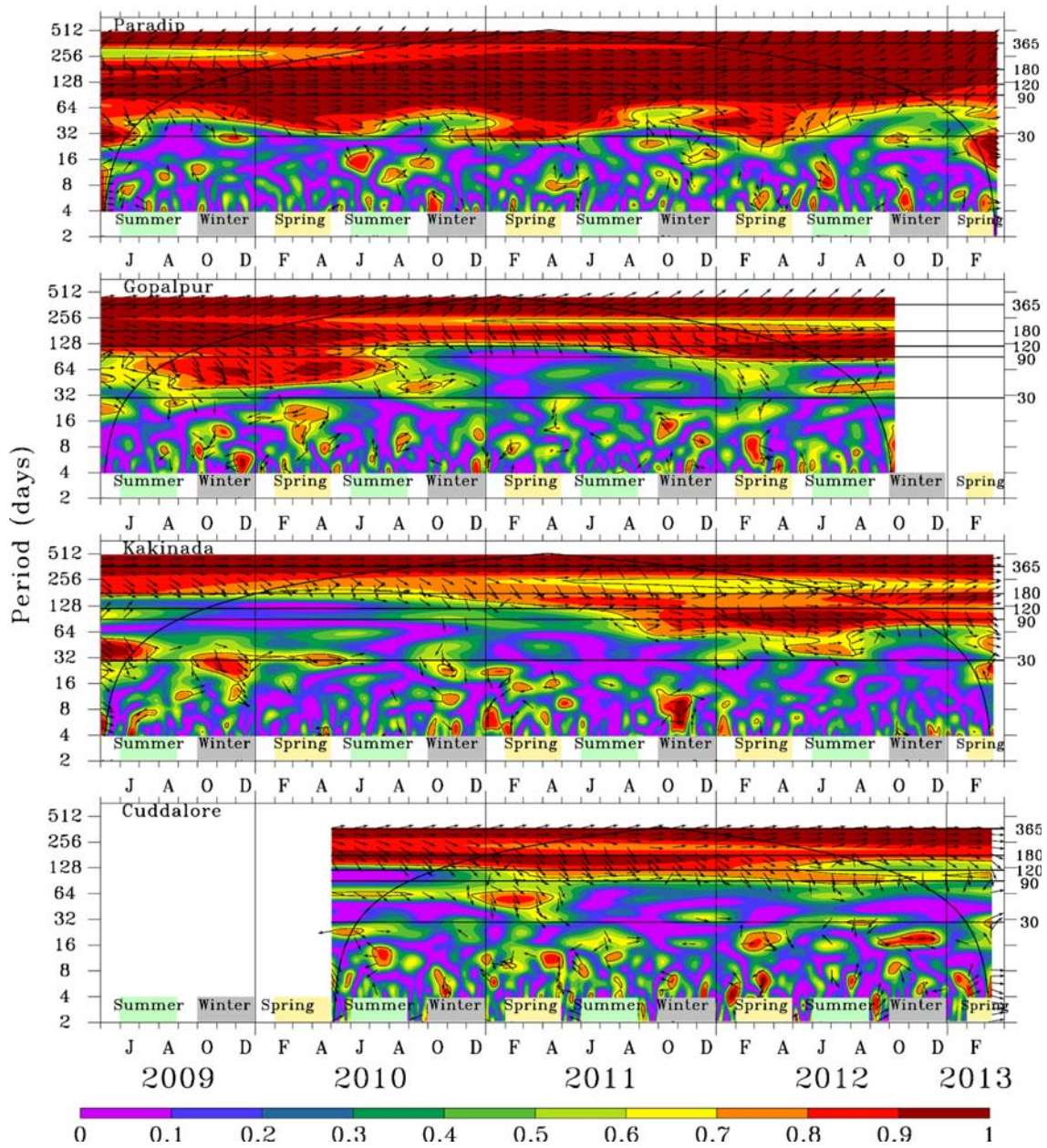


Figure 17. Wavelet coherence between ADCP and OSCAR alongshore currents. The contour line shows the 5% significance level against red noise and the thick black line shows the cone of influence (COI). The arrows show the relative phase relationship with in-phase (anti-phase) pointing right (left). The ADCP current leads (lags) the OSCAR current in anticlockwise (clockwise) direction. The arrows are shown only for wavelet coherence of 0.5 or more. Note that the ordinate (period) is plotted on a  $\log_2$  scale. The horizontal solid lines mark the 30-day, 90-day, 120-day, 180-day, and 365-day periods.

## 6. Summary and discussion

We have presented data from four ADCPs deployed on the continental slope off the Indian east coast during May 2009 to March 2013. As with the ADCP data from the slope off the Indian west coast (Amol *et al.* 2014), the 4-year record length and the sampling interval of 1 hr allow a hitherto unprecedented analysis of the variability of the EICC over a range of frequencies. Such an analysis was possible earlier for only the near-surface current with

satellite altimeter data (Durand *et al.* 2009; Cheng *et al.* 2013), but these ADCP data provide a vertical profile over the depth range 40–300 m.

### 6.1 Decorrelation of seasonal alongshore EICC

Analysis of the data shows a high coherence for the annual cycle along the coast (figure 8), but with significant phase differences. The WCA brings out this difference in phase between successive

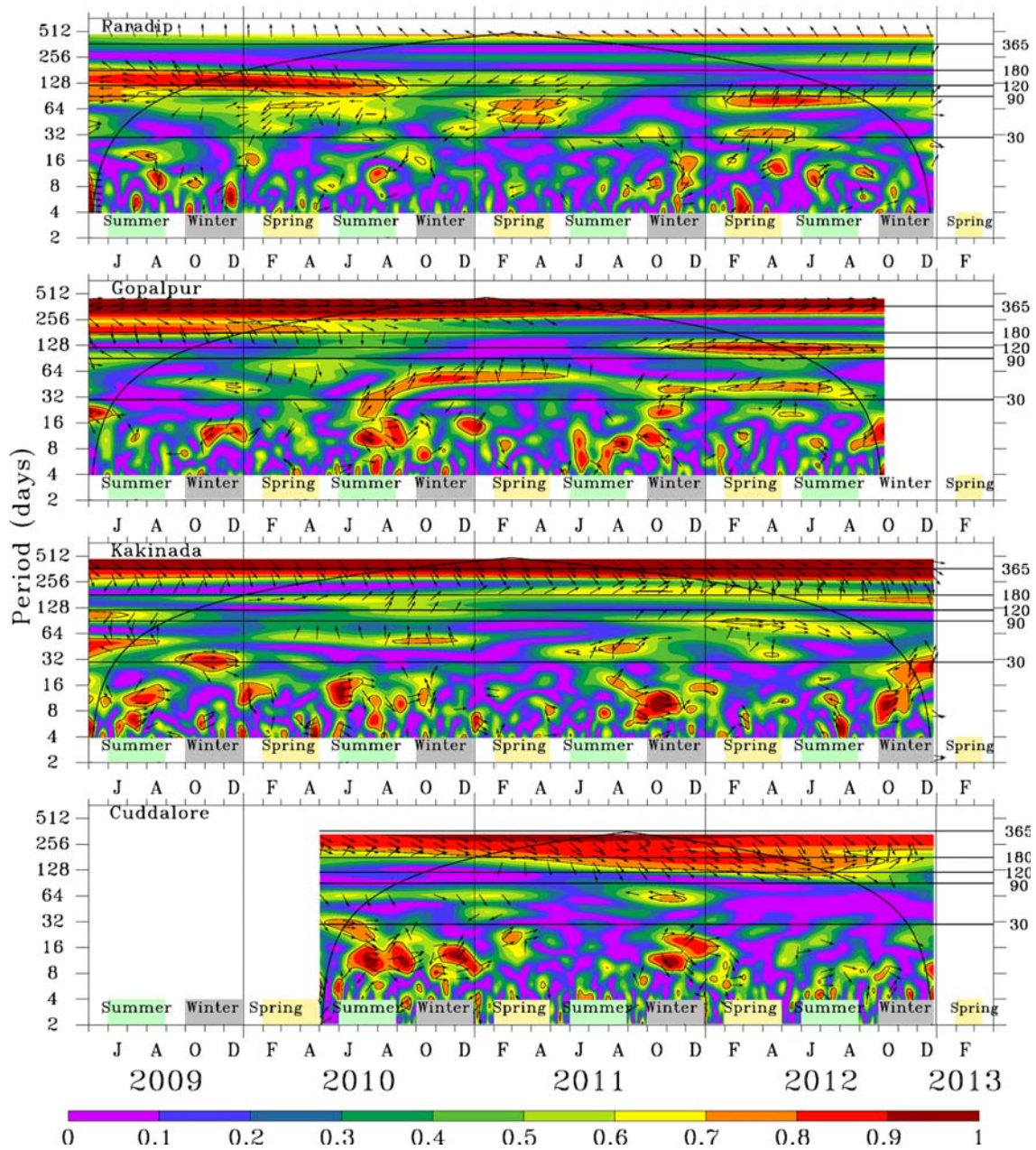


Figure 18. Wavelet coherence between ADCP and ECCO2 alongshore currents. The contour line shows the 5% significance level against red noise and the thick black line shows the cone of influence (COI). The arrows show the relative phase relationship with in-phase (anti-phase) pointing right (left). The ADCP current leads (lags) the ECCO2 current in anticlockwise (clockwise) direction. The arrows are shown only for wavelet coherence of 0.5 or more. Note that the ordinate (period) is plotted on a  $\log_2$  scale. The horizontal solid lines mark the 30-day, 90-day, 120-day, 180-day, and 365-day periods.

mooring pairs, presenting a facet of the variability that is missed when the coherence is evaluated using cross-correlations (as shown in table 4). Though it may appear that the weak coherence for the intra-annual EICC (period range 100–250 days) and large phase difference for the annual EICC suggest an alongshore decorrelation even of the seasonal cycle, we argue against such an inference. Such differences in phase are to be expected because the seasonal EICC is the resultant of

four different forcing mechanisms (McCreary *et al.* 1996; Shankar *et al.* 1996; Vinayachandran *et al.* 1996), each of which trigger long, baroclinic waves. Differences in the timing of the reversal is therefore to be expected because of the location of the moorings. The Paradip mooring lies on the continental slope of the northern bay (and at a deeper depth of  $\sim 2000$  m). Therefore, its seasonal cycle is not affected by that of the strong winds that are local to the east coast of India and Sri Lanka because

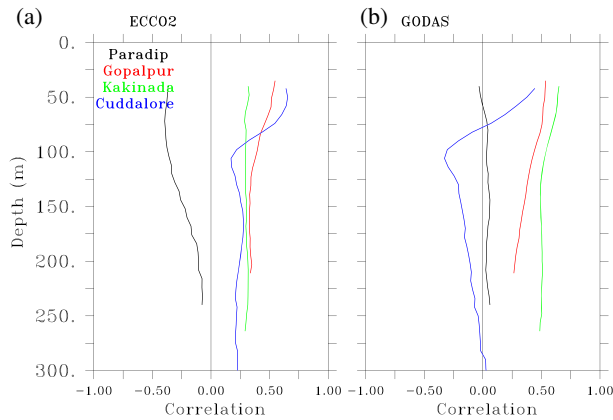


Figure 19. Correlation between alongshore currents from ADCP and (a) ECCO2 and (b) GODAS as a function of depth.

coastal Kelvin waves propagate anticlockwise along the perimeter of the bay. Since the Paradip current is forced by the other three forcing mechanisms, its phase will be determined by the interplay between them. The Gopalpur mooring lies at the northern end of the east-coast slope and is therefore at the northern edge of the east-coast wind forcing. Hence, since the east-coast response to the local winds is determined by integrating from north to south along the coast, the Gopalpur currents will not be as strongly forced by these east-coast winds as will the currents at Kakinada. This equatorward summer-monsoon EICC at the northern end of the Indian east coast, i.e., near Gopalpur, has been noted earlier in hydrographic (Shetye *et al.* 1991b) and ship-drift and sea-level (Shankar 1998, 2000) data and has been attributed to forcing from the Equator and to interior Ekman pumping (McCreary *et al.* 1993, 1996). Cuddalore's location near the 10°N separator for Ekman pumping over the bay (McCreary *et al.* 1996) leads to the weaker coherence with Kakinada. In summary, the complex interplay among the four forcing mechanisms with respect to their amplitudes and phases can produce fairly complicated patterns even in the seasonal EICC.

### 6.2 120-day variability

A striking feature of the seasonal cycle on the east coast is the strong peak around 120 days (figures 4–5). Such a peak was not prominent off the west coast, where peaks at 100–110 (140) days were seen at Mumbai (Kollam). Nethery and Shankar (2007) noted this 120-day peak in the current measurements made by Schott *et al.* (1994) off the southern tip off Sri Lanka during 1991–1992, and it has been discussed by others subsequently (Han *et al.* 2011; Cheng *et al.* 2013; Girishkumar

*et al.* 2013). What forces this 120-day peak at the mooring locations is not clear, but it dominates the seasonal cycle at Paradip in both ADCP (figure 5) and OSCAR (figure 20) data.

### 6.3 Intraseasonal variability

Intraseasonal variability in the 30–90-day band is weak at Paradip and Cuddalore, but the intraseasonal peaks at Kakinada and, to a lesser extent, Gopalpur, are significant (figure 4). This intraseasonal variability varies seasonally, peaking during spring at all locations, but, except at Paradip, variability in this band extends to the other seasons as well. Nevertheless, it is the seasonal cycle that dominates the EICC variability, unlike for the WICC (Amol *et al.* 2014). The ADCP data also show variability at subinertial periods less than 30 days, particularly at Kakinada and Gopalpur. The 12-day period noted on the west-coast shelf (Amol *et al.* 2012) and slope (Amol *et al.* 2014) is seen on the east-coast slope as well, but the 4-day band is not evident on the east coast (figure 4). A burst in the 8–12-day band at Kakinada and Cuddalore is often accompanied by near-inertial currents (figure 12), but there is a clear separation between the subinertial and near-inertial bands at Paradip and Gopalpur.

### 6.4 Upward and downward phase propagation

As seen off the west coast (Amol *et al.* 2014), there is a difference in phase between the ADCP and OSCAR currents even when the coherence exceeds 0.8 (figure 17). Amol *et al.* (2014) attributed this phase difference to upward phase propagation, which is seen on the east coast as well. This upward propagation of phase can introduce a lag between the ADCP current at 40 m (the topmost common depth level) and the surface current. OSCAR is supposed to represent the current averaged over the top 30 m. The mixed layer in the bay is shallower than 40 m at the mooring locations throughout the year (Montegut *et al.* 2004; Chatterjee *et al.* 2012) (figure 21), and it is possible that the phase continues to propagate upward till the base of the mixed layer, which is within the averaging depth range of the OSCAR currents. Therefore, we examined the current data at Gopalpur during February–October 2012, when the data are available till 24 m because the ADCP was deployed at a shallower depth on the mooring line (table 3). The 30-day low-pass-filtered current at 24 m is similar to the 40 m current in that both are in the same direction most of the time, but the magnitude range is less at 24 m (figure 22). The two

currents are in opposite directions during March–April because the equatorward current core is centred around 60 m and therefore represents an undercurrent. The result of these differences is that the 24 m current lags (leads) the 40 m current during February–March (March–April), but the weaker variability near the surface makes it difficult to decide if there is a definite change in phase from 40 to 24 m. The OSCAR current seems to match the 40 m current better, unlike on the west coast, where the difference between the 24 and 48 m ADCP currents and the OSCAR current was not as striking (Amol *et al.* 2014).

Downward propagation of phase, seen off the west coast, is seen in the east-coast moorings as well; an example is seen at Cuddalore during June 2010 to April 2011 (figure 7). A possible explanation for this downward phase propagation is the combination of vertical normal modes associated with locally and remotely forced currents.

### 6.5 Undercurrent

The upward propagation of phase led to distinct undercurrents off the west coast (Amol *et al.* 2014).

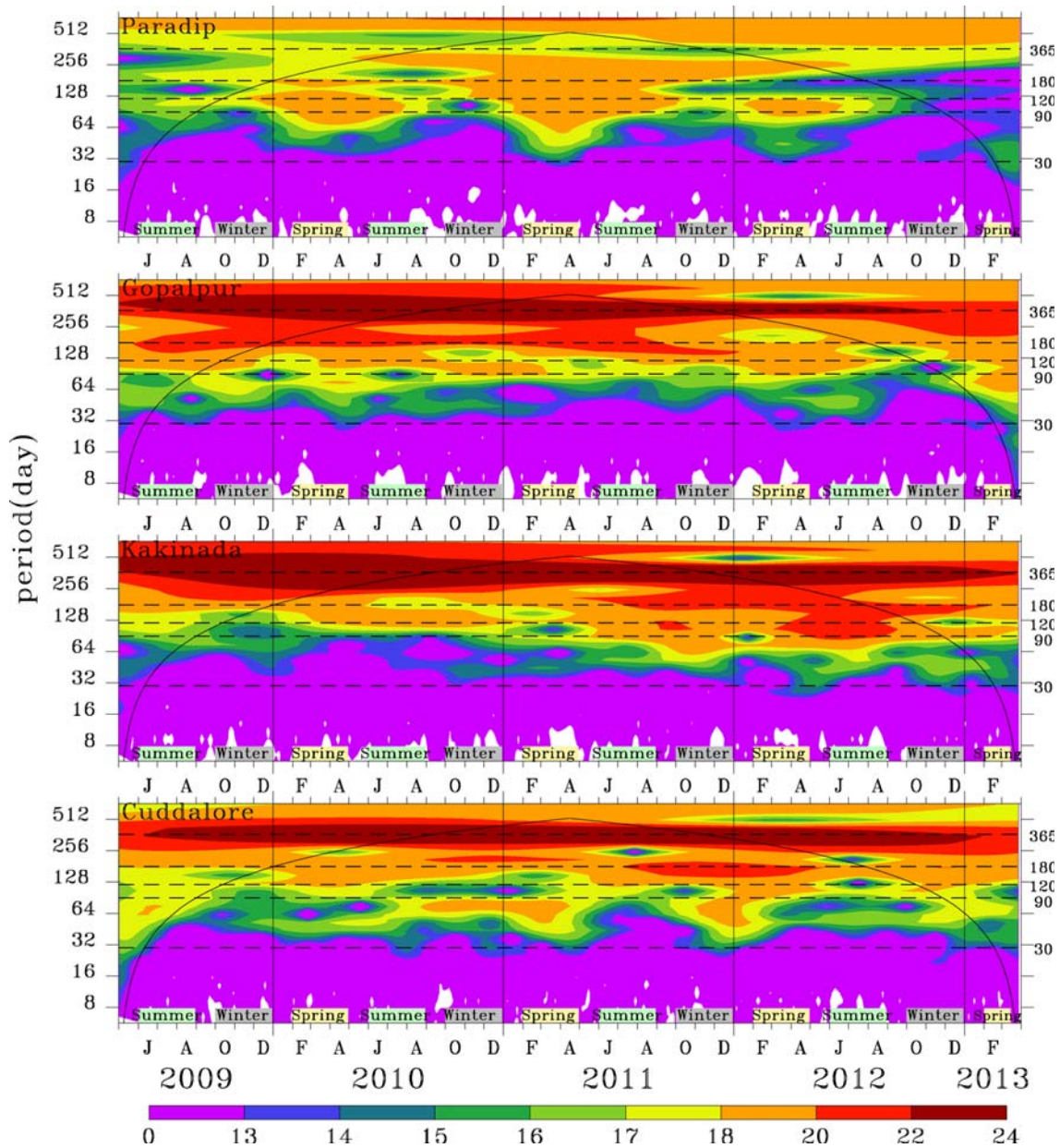


Figure 20. Morlet wavelet power spectra ( $\text{cm}^2 \text{s}^{-2}$ ) for OSCAR alongshore currents calculated at the ADCP locations. The thick black line shows the cone of influence. The ordinate and wavelet power are plotted on a  $\log_2$  scale. The horizontal dashed lines mark the 30-day, 90-day, 120-day, 180-day, and 365-day periods. Note that the colour scale is not uniform.

Off the east coast and at the Paradip mooring, however, the vertical phase speed is much higher compared to the west coast, the only exception being the much slower phase propagation in the top 100 m at Cuddalore (figure 6). As a result, a distinct undercurrent is seen only at Cuddalore over most of the year; at other locations, the current is unidirectional over the top 300 m during spring, but an undercurrent does tend to form during the

summer monsoon and winter. However, we note that the ADCPs do not sample the top  $\sim 40$  m, and the short Gopalpur record with measurements till 24 m suggests that there can be occasions on which the surface current may even be directed opposite to that at 40 m.

### 6.6 Cross-shore currents

Off the west coast, strong cross-shore currents were found at Kollam and Kanyakumari, the two southernmost locations; the weakening of the cross-shore current at Goa and Mumbai farther north was attributed to the smaller length scale, the Rossby radius of deformation, at these locations (Amol *et al.* 2014). In contrast, off the east coast, the cross-shore currents are weakest at Cuddalore, the southernmost location (figures 13 and 15). Cross-shore flows occur in bursts, typically during spring, at Kakinada and Gopalpur. It is only at Paradip, the northernmost location and therefore the one with the smallest length scale, that the cross-shore component is often comparable to the alongshore component during spring and the summer monsoon (figure 14). Examination of the altimeter sea level suggests that such strong cross-shore flows are associated with eddy-like circulations (figure 23); the correlation between the cross-shore currents estimated from ADCP measurements and OSCAR data are, however, weak (table 4).

### 6.7 Ocean current data products

A comparison between currents from the ADCPs and the OSCAR data product shows that the latter is able to capture both seasonal and intraseasonal variability only for the Paradip mooring, where the match is remarkably good (figures 16–17). At the other three locations, which are on the continental slope of the western boundary, the OSCAR currents are able to capture only the seasonal variability; the match at intraseasonal periods is reasonable, but there are several intraseasonal bursts that are seen in the ADCP data, but not in OSCAR. A wavelet analysis of the OSCAR data at the four locations (figure 20) shows similarities with the ADCP wavelet spectrum (figure 5), but there are also significant differences. A WCA analysis for the OSCAR data from the mooring locations (figure 24) leads to results similar to the ADCP WCA (figure 8).

Apart from OSCAR, we validated the currents estimated from two model-based data products, ECCO2 and GODAS. As found off the west coast (Amol *et al.* 2014), the variability simulated by GODAS is weak, but ECCO2 fares better at the

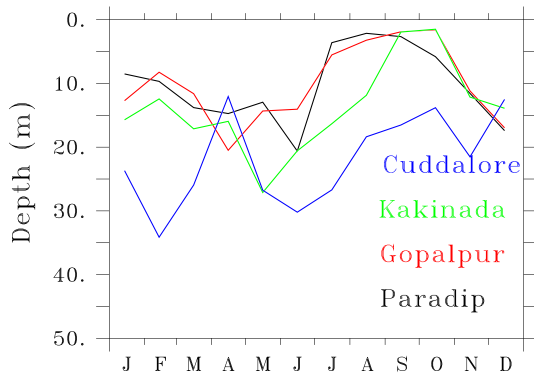


Figure 21. Climatology of mixed layer depth (m) based on Chatterjee *et al.* (2012) at the ADCP locations. The mixed layer depth is assumed to be the depth at which the density exceeds the surface density by  $0.2 \text{ kg m}^{-3}$ .

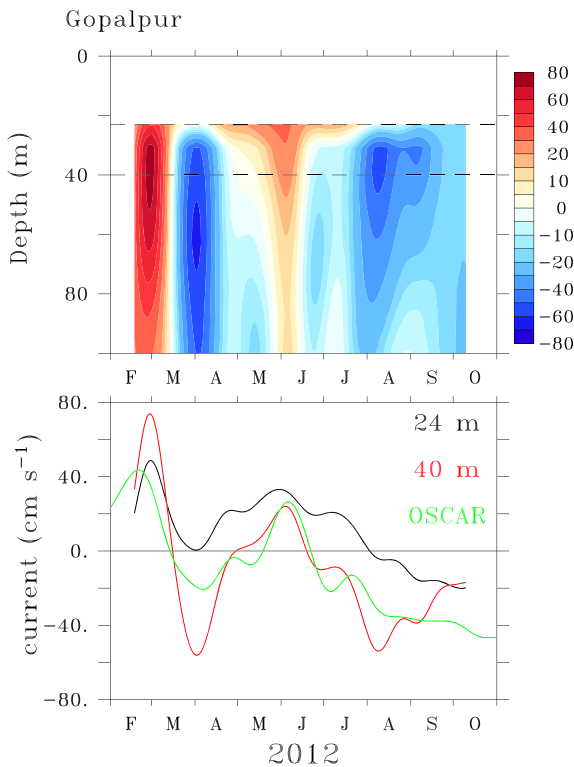


Figure 22. The top panel shows the 30-day low-passed currents as a function of depth at Gopalpur. The dashed horizontal lines mark the 24 m and 40 m water depth. The bottom panel shows the same 30-day low-passed currents at 24 m and 40 m and for the OSCAR product.

three locations on the east-coast slope (figure 16). It is only at Paradip that the ECCO2 simulation is really poor; at the other locations, the coherence is fairly good for the annual cycle, but the ECCO2 current is not in phase with the ADCP current (figure 18), leading to a poor correlation (table 4). At the intra-annual and intraseasonal periods, however, ECCO2 shows a match with the ADCP only on occasions at Gopalpur. Both model data products fail to capture the observed variability with depth as well (figure 19).

A key reason for the poor match between these data products and direct current measurements is likely to be the coarse model resolution (Johnson *et al.* 2007; Amol *et al.* 2014). GODAS has a horizontal resolution of  $1^\circ$ , which is too coarse for resolving the characteristic cross-shore length scale, the Rossby radius of deformation, of even the gravest baroclinic mode off the east coast of India. The Rossby radius for the first vertical mode varies from  $\sim 60$  km at Paradip and Gopalpur to  $\sim 100$  km at Cuddalore. Even ECCO2, with a horizontal resolution of  $0.25^\circ$ , can barely resolve the first mode length scale at Paradip. As noted by Amol *et al.* (2014), this poor resolution of the WBC of the basin has implications for any budget estimates based on these model products (see, for example, Chacko *et al.* 2012; Rao *et al.* 2012; Wu *et al.* 2012). The Indian National Centre for Ocean Information Services (INCOIS) has recently set up a higher-resolution version of the GODAS model for the Indian-Ocean Forecasting system (INDOFOS), but it too has a  $0.5^\circ$  resolution in the regime of the EICC (Ravichandran *et al.* 2013). It will be interesting to compare the INCOIS GODAS output with the ADCP observations described here to see if it performs better than the global GODAS

product. The resolution of the INDOFOS models is being improved (Francis *et al.* 2013), however, and it will be interesting to compare the high-resolution simulations with the ADCP data to see if improving resolution is sufficient to capture the observed variability.

### 6.8 Epilogue

These ADCP data are expected to provide a fillip to theoretical studies of intraseasonal variability, just as the hydrographic data in the Indian EEZ (Shetye *et al.* 1990, 1991a, b, 1993, 1996; Shetye and Gouveia 1998) did for the seasonal cycle of circulation in the 1990s. The changes in phase seen between adjacent moorings even for the annual cycle will provide the modelling community with a dataset to test the quantitative skills of the models even for the low-frequency variability. At intraseasonal time scales, the EICC decorrelates even more strongly along the coast and the comparison with data-assimilated model products like ECCO2 and GODAS shows that the models have a long way to go before they can simulate the variability observed in the EICC.

As noted by Amol *et al.* (2014), one possible reason for the alongshore decorrelation of currents is vertical propagation of energy in the form of coastal beams. Upward propagation of phase implies downward propagation of energy and theoretical studies in the equatorial (McCreary 1984) and continental-slope regimes (Nethery and Shankar 2007) suggest that energy can propagate down into the deep ocean in the form of beams. At intraseasonal periods, the bending can be considerable: the vertical extent can be of the order

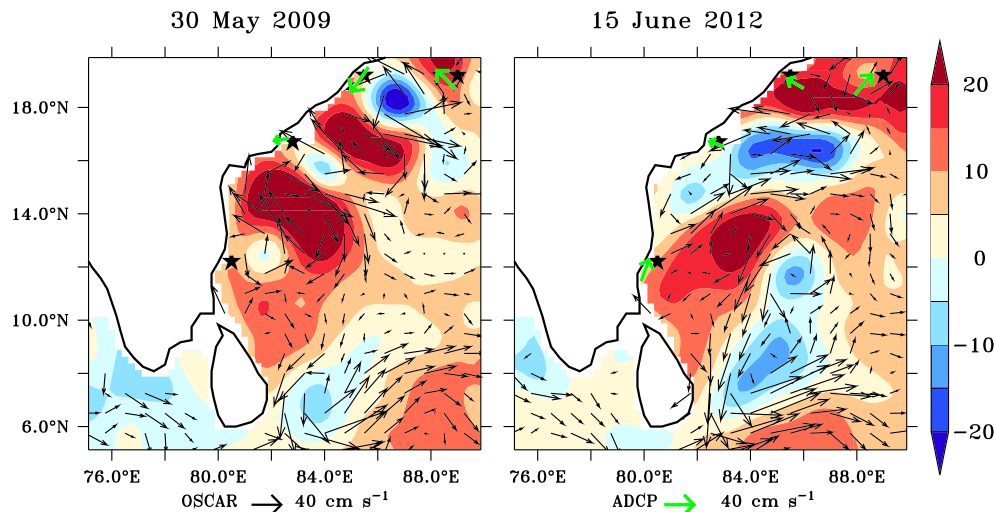


Figure 23. OSCAR currents and sea-level anomalies from altimeter (AVISO 1996) for (a) 30 May 2009 and (b) 15 June 2012. The thick green arrows show the ADCP current vectors.

of 500 m over a distance of  $\sim 1000$  km for a period of 30 days (Nethery and Shankar 2007). Unfortunately, the ADCP data are restricted to the top  $\sim 300$  m of the water column, precluding a conclusive statement on whether the vertical phase propagation will occur at greater depths as well. As noted by Amol *et al.* (2014), it is important to extend the ADCP measurements to the entire water column to map the intraseasonal variability, and the moorings are therefore being augmented to enable measurement of the complete vertical profile of currents.

The observations are continuing and a long time series of direct current measurements will allow an evaluation of the impact on the EICC of the major climate modes of the NIO (see, for example, Schott *et al.* 2009), i.e., ENSO (El Niño and Southern Oscillation) (Philander 1983; Meyers *et al.* 2007) and the IOD (Indian Ocean Dipole) (Saji *et al.* 1999; Webster *et al.* 1999). Earlier studies, typically based on altimeter data, suggest that both ENSO (Clarke and Liu 1994; Somayajulu *et al.* 2003; Aparna *et al.* 2012) and IOD (Rao *et al.* 2002; Jensen 2007; Aparna *et al.* 2012) have

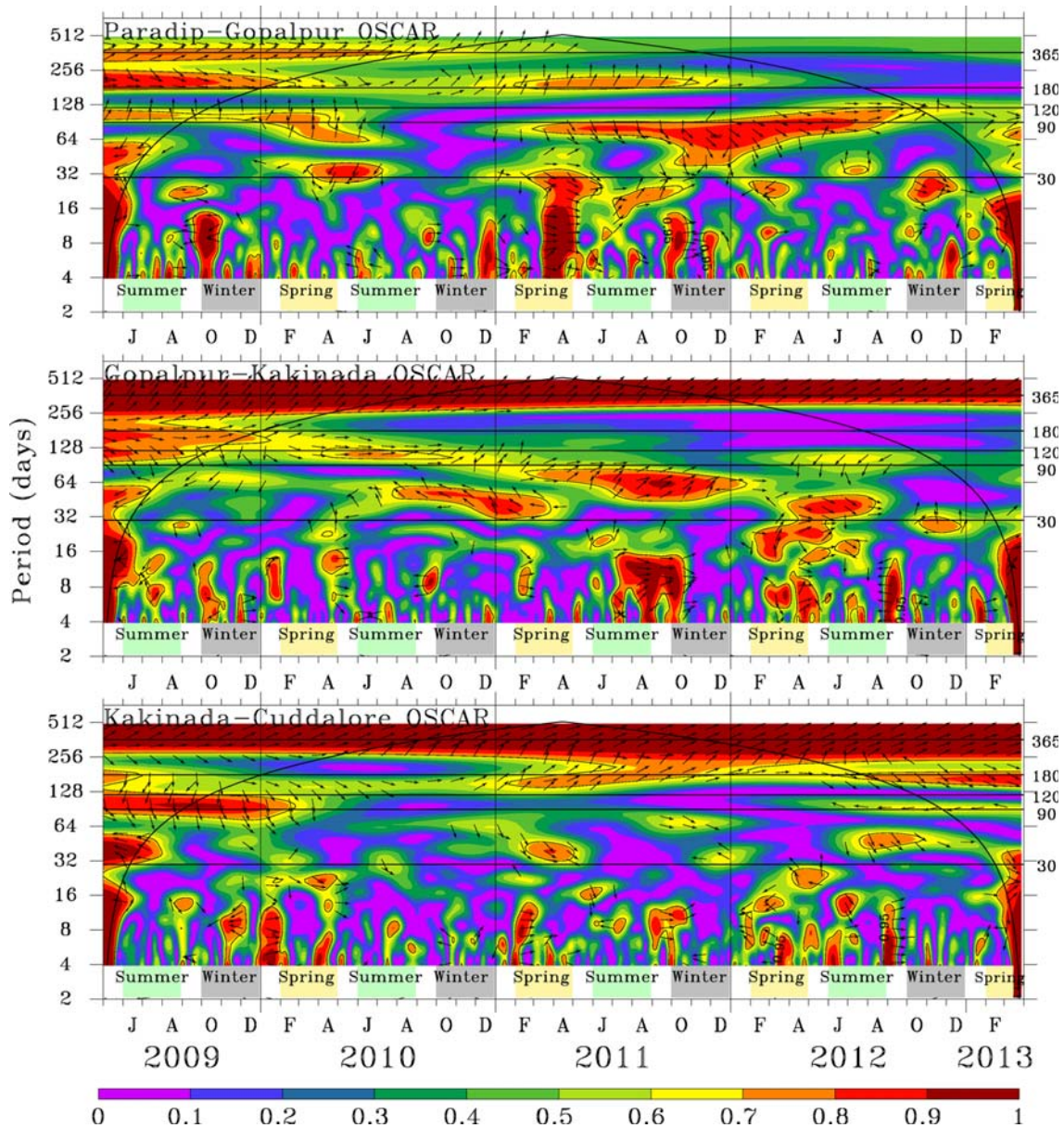


Figure 24. Wavelet coherence for the OSCAR currents at ADCP locations. The contour line shows the 5% significance level against red noise and the thick black line shows the cone of influence (COI). The arrows show the relative phase relationship with in-phase (anti-phase) pointing right (left). The first station leads (lags) the second station in anticlockwise (clockwise) direction. The arrows are shown only for wavelet coherence of 0.5 or more. Note that the ordinate (period) is plotted on a  $\log_2$  scale. The horizontal solid lines mark the 30-day, 90-day, 120-day, 180-day, and 365-day periods.

an impact on the western boundary of the Bay of Bengal. Another interesting question is whether a long time series of direct current measurements will show the minimum of interannual variability noted in altimeter sea level by Shankar *et al.* (2010) along the southern part of the western boundary of the bay. Along the northern part of this boundary, there was a maximum of interannual variability. Will this distinction be seen in the ADCP data? This question is important because such a difference in the variability will lead to an alongshore decorrelation of the interannual EICC, as found by Durand *et al.* (2009) using the MAP altimeter dataset in contrast to the study of Clarke and Liu (1994), who used tide-gauge data to suggest that the EICC should be coherent along the coast at these subseasonal time scales.

### Acknowledgements

The ECCO2 current data were provided by the ECCO Consortium for Estimating the Circulation and Climate of the Ocean funded by the National Oceanographic Partnership Program (NOPP) and downloaded from <http://ecco2.jpl.nasa.gov/products/>. The GODAS data were downloaded from <http://www.esrl.noaa.gov/psd/> and were provided by the NOAA/OAR/ESRL PSD, Boulder, Colorado, USA. The OSCAR current data were provided by the Physical Oceanography DAAC of the Jet Propulsion Laboratory and downloaded from <http://www.oscar.noaa.gov/>. The AVISO altimeter data were downloaded from <http://www.aviso.oceanobs.com/duacs/>. The FORTRAN code for wavelet analysis and the R package for wavelet coherence spectra were downloaded from <http://paos.colorado.edu/research/wavelets> and <http://tocsy.agnld.uni-potsdam.de/wavelets>, respectively. All figures were made using Ferret. Authors thank the officers and crew of the mooring cruises and the vessel managers of CRV *Sindhu Sankalp* and ORV *Sagar Nidhi* for their support during deployment and recovery of ADCPs. They also thank CSIR–NIO’s research vessel management group for their support. This work was supported by grants from the Council of Scientific and Industrial Research (CSIR) (under the Supra-Institutional Programme of CSIR–NIO in the XI Plan and under OCEAN FINDER in the XII Plan) and the Ministry of Earth Sciences (MoES) via the Indian National Center for Ocean Information Services (INCOIS). A Mukherjee thanks both CSIR and MoES for his research funding. Finally, authors acknowledge the critical comments from two anonymous reviewers, which helped improve the manuscript. This is NIO contribution 5578.

### References

- Ali M M, Sharma R and Cheney R 1998 An atlas of the north Indian Ocean eddies from TOPEX altimeter derived sea surface heights; *Indian Space Research Organization (ISRO) Special Publication*, pp. 69–98.
- Amol P, Shankar D, Aparna S G, Shenoi S S C, Fernando V, Shetye S R, Mukherjee A, Agarvadekar Y, Khalap S and Satelkar N P 2012 Observational evidence from direct current measurements for propagation of remotely forced waves on the shelf off the west coast of India; *J. Geophys. Res.* **117** C05017, doi: [10.1029/2011JC007606](https://doi.org/10.1029/2011JC007606).
- Amol P, Shankar D, Fernando V, Mukherjee A, Aparna S G, Fernandes R, Michael G S, Khalap S T, Satelkar N P, Agarvadekar Y, Gaonkar M G, Tari A P, Kankonkar A and Vernekar S P 2014 Observed intraseasonal and seasonal variability of the West India Coastal Current on the continental slope; *J. Earth Syst. Sci.* **123**(5) 1045–1074.
- Aparna S G, McCreary J P, Shankar D and Vinayachandran P N 2012 Signatures of the Indian Ocean Dipole and El Niño–Southern Oscillation events in sea level variations in the Bay of Bengal; *J. Geophys. Res.* **117** C10012, doi: [10.1029/2012JC008055](https://doi.org/10.1029/2012JC008055).
- AVISO 1996 AVISO User Handbook; *Technical Report*. Toulouse, France.
- Babu M T, Sarma Y V B, Murthy V S N and Vethamony P 2003 On the circulation in the Bay of Bengal during northern spring inter-monsoon (March–April 1987); *Deep-Sea Res. (Part II)* **5** 855–865, doi: [10.1016/S0967-0645\(02\)00609-4](https://doi.org/10.1016/S0967-0645(02)00609-4).
- Behringer D W 2007 The Global Ocean Data Assimilation System (GODAS) at NCEP; *11th Symp. on Integrated Observing and Assimilation Systems for Atmosphere, Oceans, and Land Surface* 3.3, Amer. Meteor. Soc., San Antonio, TX.
- Behringer D W and Xue Y 2004 Evaluation of the global ocean data assimilation system at NCEP: The Pacific Ocean; *Eighth Symposium on Integrated Observing and Assimilation Systems for Atmosphere, Oceans, and Land Surface* **2.3** 11–15, Amer. Meteor. Soc. Washington State Convention and Trade Center, Seattle, Washington.
- Behringer D W, Ji M and Leetmaa A 1998 An improved coupled model for ENSO prediction and implications for ocean initialization. Part I: The ocean data assimilation system; *Mon. Wea. Rev.* **126** 1013–1021.
- Bell C, Vassie J and Woodworth P 1998 POL-PSMSL Tidal Analysis Software Kit 2000 (TASK-2000), Technical Report; Proudman Oceanogr. Lab Bidston Obs Merseyside, UK.
- Birol F, Roblou L, Lyard F, Llovel W, Durand F, Renault L, Dewitte B, Morrow R and Mnard Y 2006 Towards using satellite altimetry for the observation of coastal dynamics; In: *15 Years of Progress in Radar Altimetry Symposium*, Venice, Italy.
- Bonjean F and Lagerloef G S E 2002 Diagnostic model and analysis of the surface currents in the tropical Pacific Ocean; *J. Phys. Oceanogr.* **32** 2938–2954.
- Bruce J G, Johnson D R and Kindle J C 1994 Evidence for eddy formation in the eastern Arabian Sea during the northeast monsoon; *J. Geophys. Res.* **99** 7651–7664.
- Bruce J G, Kindle J C, Kantha L H, Kerling J L and Bailey J F 1998 Recent observations and modeling in the Arabian Sea Laccadive high region; *J. Geophys. Res.* **103** 7593–7600.
- Chacko N, Ravichandran M, Rao R R and Shenoi S S C 2012 An anomalous cooling event observed in the Bay



- of Bengal during June 2009; *Ocean Dynam.* **62** 671–681, doi: [10.1007/s10236-012-0525-9](https://doi.org/10.1007/s10236-012-0525-9).
- Chatterjee A, Shankar D, Shenoi S S C, Reddy G V, Michael G S, Ravichandran M, Gopalakrishna V V, Rao E P R, Bhaskar T V S U and Sanjeevan V N 2012 A new atlas for temperature and salinity for north Indian Ocean; *J. Earth Syst. Sci.* **121**(3) 559–593.
- Chen G, Wang D and Hou Y 2012 The features and interannual variability mechanism of mesoscale eddies in the Bay of Bengal; *Cont. Shelf. Res.* **47** 178–185.
- Cheng X, Xie S P, McCreary J P, Qi Y and Du Y 2013 Intraseasonal variability of sea surface height over the Bay of Bengal; *J. Geophys. Res.* **118** 1–15, doi: [10.1002/jgrc.20075](https://doi.org/10.1002/jgrc.20075).
- Chinthalu G R, Seetaramayya P, Ravichandran M and Mahajan P N 2002 The Bay of Bengal and tropical cyclones; *Curr. Sci.* **82** 379–381.
- Clarke A J and Liu X 1994 Interannual sea level in the northern and eastern Indian Ocean; *J. Phys. Oceanogr.* **24** 1224–1235, doi: [10.1017/1520-0485](https://doi.org/10.1017/1520-0485).
- Cutler A N and Swallow J C 1984 Surface currents of the Indian ocean; Technical report. **187**, Inst. of Oceanogr. Sci., Wormley, England.
- Derber J and Rosati A 1989 A global oceanic data assimilation system; *J. Phys. Oceanogr.* **19** 1333–1347.
- Dileepkumar M 2006 Biogeochemistry of the North Indian Ocean; *IGBP-WCRP-SCOPE Rep. Ser. 1*, Indian Nat. Sci. Acad., New Delhi, India.
- Durand F, Shankar D, de B Montegut C and Shenoi S S C 2008 Estimating boundary currents from satellite altimetry: A case study for the east coast of India; *J. Oceanogr.* **64** 831–845, doi: [10.1007/s10872-008-0069-2](https://doi.org/10.1007/s10872-008-0069-2).
- Durand F, Shankar D, Birol F and Shenoi S S C 2009 Spatiotemporal structure of the East India Coastal Current from satellite altimetry; *J. Geophys. Res.* **114** CO2013, doi: [10.1029/2008JC004807](https://doi.org/10.1029/2008JC004807).
- Eigenheer A and Quadfasel D 2000 Seasonal variability of the Bay of Bengal circulation inferred from TOPEX/Poseidon altimetry; *J. Geophys. Res.* **105** 3243–3252.
- Francis P A, Vinayachandran P N and Shenoi S S C 2013 The Indian ocean forecast system; *Curr. Sci.* **104**(10) 1354–1368.
- Gangopadhyay A, Bharatraj G N, Chaudhuri A H, Babu M T and Sengupta D 2013 On the nature of meandering of the springtime western boundary current in the Bay of Bengal; *Geophys. Res. Lett.* **40** 2188–2193, doi: [10.1002/grl.50412](https://doi.org/10.1002/grl.50412).
- Girishkumar M S, Ravichandran M and Han W 2013 Observed intraseasonal thermocline variability in the Bay of Bengal; *J. Geophys. Res.* **118** 1–14, doi: [10.1002/jgrc.20245](https://doi.org/10.1002/jgrc.20245).
- Gopalan A K S, Gopalakrishna V V, Ali M M and Sharma R 2000 Detection of BoB eddies from TOPEX and sea truth observations; *J. Mar. Res.* **58** 721–734.
- Han W and McCreary J P 2002 Modeling salinity distributions in the Indian Ocean; *J. Geophys. Res.* **106** 859–877.
- Han W and Webster P 2002 Forcing mechanisms of sea level inter-annual variability in the Bay of Bengal; *J. Phys. Oceanogr.* **32** 216–239.
- Han W, McCreary J P, Anderson D L T and Mariano A J 1999 On the dynamics of the eastward surface jets in the equatorial Indian Ocean; *J. Phys. Oceanogr.* **29** 2191–2209.
- Han W, Lawrence D M and Webster P J 2001a Dynamical response of equatorial Indian Ocean to intraseasonal winds: zonal flow; *Geophys. Res. Lett.* **28** 4215–4218.
- Han W, McCreary J P and Kohler K 2001b Influence of precipitation minus evaporation and Bay of Bengal rivers on dynamics, thermodynamics and mixed-layer physics in the upper Indian Ocean; *J. Geophys. Res.* **106** 6895–6916, doi: [10.1029/2000JC000403](https://doi.org/10.1029/2000JC000403).
- Han W, McCreary J P, Masumoto Y, Vialard J and Duncan B 2011 Basin resonances in the equatorial Indian Ocean; *J. Phys. Oceanogr.* **41** 1252–1270.
- Hurlburt H E, Kindle J C and O'Brien J J 1976 A numerical simulation of the onset of El Niño; *J. Phys. Oceanogr.* **6** 621–631.
- Jensen T G 1993 Equatorial variability and resonance in a wind-driven Indian Ocean model; *J. Geophys. Res.* **98** 22,533–22,552.
- Jensen T G 2007 Wind-driven response of the northern Indian Ocean to climate extremes; *J. Climate* **20** 2978–2993, doi: [10.1175/JCLI4150.1](https://doi.org/10.1175/JCLI4150.1).
- Johnson E S, Bonjean F, Lagerloef G S E and Gunn J T 2007 Validation and error analysis of OSCAR sea surface currents; *J. Atmos. Ocean Tech.* **24** 688–701.
- Joseph K J, Balchand A N, Hareeshkumar P and Rajesh G 2006 Inertial oscillation forced by the September 1997 cyclone in the Bay of Bengal; *Curr. Sci.* **92** 790–794.
- KNMI 1952 Indische Ocean Oceanographische en Meteorologische Oegevans; 2nd edn, 24 charts.
- Kumar S P, Nuncio M, Narvekar J, Kumar A, Sardesai S, de Souza S N, Gauns M, Ramaiah N and Madhupratap M 2004 Are eddies nature's trigger to enhance biological productivity in the Bay of Bengal? *Geophys. Res. Lett.* **31** L07309, doi: [10.1029/2003GL019274](https://doi.org/10.1029/2003GL019274).
- Kumar S P, Nuncio M, Ramaiah N, Sardesai S, Narvekar J, Veronica F and Jane T P 2007 Eddy-mediated biological productivity in the Bay of Bengal during fall and spring intermonsoons; *Deep-Sea Res. (Part I)* **54** 1619–1640, doi: [10.1016/j.dsr.2007.06.002](https://doi.org/10.1016/j.dsr.2007.06.002).
- Kurian P, Ikeda M and Valsala V K 2010 Mesoscale variability along the east coast of India in spring as revealed from satellite data and OGCM simulations; *J. Oceanogr.* **66** 273–289, doi: [10.1007/s10872-010-0024-x](https://doi.org/10.1007/s10872-010-0024-x).
- Kutsuwada K and McPhaden M 2002 Intraseasonal variations in the upper Equatorial Pacific Ocean prior to and during the 1997–98 El-Niño; *J. Phys. Oceanogr.* **32** 1133–1149.
- Legeckis R 1987 Satellite observations of a western boundary current in the Bay of Bengal; *J. Geophys. Res.* **92** 12,974–12,978.
- Madden R A and Julian P R 1971 Detection of a 40–50 day oscillation in the zonal wind of the tropical Pacific; *J. Atmos. Sci.* **28** 702–708.
- Madden R A and Julian P R 1972 Description of global-scale circulation cells in the tropics with a 40–50 day period; *J. Atmos. Sci.* **29** 1109–1123.
- Madden R A and Julian P R 1993 Observations of the 40–50 day tropical oscillation – A review; *Mon. Wea. Rev.* **122** 814–837.
- Madhupratap M, Gauns M, Ramaiah N, Kumar S P and Muraleedharan P M 2003 Biogeochemistry of the Bay of Bengal: Physical, chemical and primary productivity characteristics of the central and western Bay of Bengal during summer monsoon 2001; *Deep-Sea Res. (Part II)* **50** 881–896.
- Mariano A J, Ryan E H, Perkin B D and S S 1995 The Mariano Global Surface Velocity Analysis; *US Coast Guard, Washington* 1.0, Rep CG–D–34–95 55p.
- Marshall J, Adcroft A, Hill C, Perelman L and Heisey C 1997 A finite-volume, incompressible Navier–Stokes model for studies of the ocean on parallel computers; *J. Geophys. Res.* **102** 5753–5766, doi: [10.1029/96JC02775](https://doi.org/10.1029/96JC02775).

- McCreary J P 1976 Eastern tropical ocean response to changing wind systems: With application to El Niño; *J. Phys. Oceanogr.* **6** 632–645.
- McCreary J P 1984 Equatorial beams; *J. Mar. Res.* **42** 395–430.
- McCreary J P, Picaut J and Moore D W 1984 Effects of remote annual forcing in the eastern tropical Atlantic Ocean; *J. Mar. Res.* **42** 45–81.
- McCreary J P, Kundu P K and Molinari R L 1993 A numerical investigation of dynamics, thermodynamics and mixed-layer processes in the Indian Ocean; *Prog. Oceanogr.* **31** 181–244.
- McCreary J P, Han W, Shankar D and Shetye S R 1996 Dynamics of the East India Coastal Current 2. Numerical solutions; *J. Geophys. Res.* **101** 13,993–14,010.
- McCreary J P, Murtugudde R, Vialard J, Vinayachandran P N, Wiggert J D, Hood R R, Shankar D and Shetye S 2009 Biophysical processes in the Indian Ocean; *Geophys. Monogr. Series* **185** 9–32.
- McPhaden M J, Meyers G, Ando K, Masumoto Y, Murty V S N, Ravichandran M, Syamsudin F, Vialard J, Yu L and Yu W 2009 RAMA The research moored array for African–Asian–Australian monsoon analysis and prediction a new moored buoy array in the historically data-sparse Indian Ocean provides measurements to advance monsoon research and forecasting; *Bull. Am. Meteorol. Soc.* **90** 459–480, doi: [10.1175/2008BAMS2608.1](https://doi.org/10.1175/2008BAMS2608.1).
- Menemenlis D, Hill C, Adcroft A, Campin J, Cheng B, Ciotti B, Fukumori I, Koehl A, Heimbach P, Henze C, Lee T, Stammer D, Taft J and Zhang J 2005 NASA supercomputer improves prospects for ocean climate research; *EOS Trans. AGU* **86** 86–89.
- Meyers G, McIntosh P, Pigot L and Pook M 2007 The years of El Niño, La Niña, and interactions with the tropical Indian Ocean; *J. Climate* **20** 2872–2880.
- Mishra P, Patra S K, Ramanamurthy M V, Mohanty P K and Panda U S 2011 Interaction of monsoonal wave, current and tide near Gopalpur, east coast of India, and their impact on beach profile: A case study; *Nat. Hazards* **59** 1145–1159.
- Molinari R L, Olson D and Reverdin G 1990 Surface current distributions in the tropical Indian Ocean derived from compilations of surface buoy trajectories; *J. Geophys. Res.* **95** 7217–7238.
- Montegut C D B, Madee G, Fischer A S, Lazar A and Iudicone D 2004 Mixed layer depth over the global ocean: An examination of profile data and a profile based climatology; *J. Geophys. Res.* **109** C12003, doi: [10.1029/2004JC002378](https://doi.org/10.1029/2004JC002378).
- Moore D W 1968 Planetary-gravity waves in an Equatorial Ocean; Ph.D thesis, Harvard University.
- Mukherjee A, Shankar D, Aparna S G, Amol P, Fernando V, Fernandes R, Khalap S, Narayan S, Agarvadekar Y, Gaonkar M, Tari P, Kankonkar A and Vernekar S 2013 Near-inertial currents off the east coast of India; *Cont. Shelf Res.* **55** 29–39, doi: [10.1016/j.csr.2013.01.007](https://doi.org/10.1016/j.csr.2013.01.007).
- Murty B C 1958 On the temperature and salinity structure of the Bay of Bengal; *Curr. Sci.* **27** 249.
- Murty V S N, Suryanarayana A and Rao D P 1993 Current structure and volume transport across 12°N in the Bay of Bengal; *Indian J. Mar. Sci.* **22** 12–16.
- Naqvi S W, Narvekar P V and Desa E 2006 Coastal biogeochemical processes in the North Indian Ocean (14, S-W); *The Sea* **14** 723–780.
- Nethery D and Shankar D 2007 Vertical propagation of baroclinic Kelvin waves along the west coast of India; *J. Earth Syst. Sci.* **116** 331–339.
- Nuncio M and Kumar S P 2012 Life cycle of eddies along the western boundary of the Bay of Bengal and their implications; *J. Marine Syst.* **94** 9–17.
- O’Brien J J, Adamec D and Moore D W 1978 A simple model of upwelling in the Gulf of Guinea; *Geophys. Res. Lett.* **5** 641–644, doi: [10.1029/GL005i008p00641](https://doi.org/10.1029/GL005i008p00641).
- Pacanowski R C and Griffies S M 1998 *MOM 3.0 Manual*; NOAA/Geophysical Fluid Dynamics Laboratory; Princeton, USA 08542.
- Pandey V K and Singh S K 2010 Comparison of ECCO2 and NCEP reanalysis using TRITON and RAMA data at the Indian Ocean Mooring Buoy point; *Earth Sci. India* **3(IV)** 226–241.
- Philander S G H 1983 El Niño Southern Oscillation phenomena; *Nature* **302** 295–301.
- Picaut J 1983 Propagation of seasonal coastal upwelling in the eastern equatorial Atlantic; *J. Phys. Oceanogr.* **13** 18–37.
- Potemra J T, Luther M E and O’Brien J J 1991 The seasonal circulation of the upper ocean in the Bay of Bengal; *J. Geophys. Res.* **96** 12,667–12,683, doi: [10.1029/91JC01045](https://doi.org/10.1029/91JC01045).
- Rao T V N 2002 Spation distribution of upwelling off the central east coast of India; *Estuarine Coast. Shelf Sci.* **54** 141–156.
- Rao T V N 2004 Flow field in the inner shelf along the Central East Coast of India during the southwest monsoon season; *J. Coastal Res.* **20** 814–827.
- Rao R R, Molinari R L and Festa J F 1991 Surface meteorological and near surface oceanographic atlas of the tropical Indian Ocean; *NOAA-Tech. Memo. ERL, AOML-69*.
- Rao S, Behera S K, Masumoto Y and Yamagata T 2002 Inter-annual subsurface variability in the tropical Indian Ocean with a special emphasis on the Indian Ocean Dipole; *Deep-Sea Res. (Part II)* **49** 1549–1572.
- Rao R R, Kumar M S G, Ravichandran M, Rao A R, Gopalakrishna V V and Thadathil P 2009 Interannual variability of Kelvin wave propagation in the wave guides of the equatorial Indian Ocean, the coastal Bay of Bengal and the southeastern Arabian Sea during 1993–2006; *Deep-Sea Res. (Part I)* **57** 1–13.
- Rao S A, Dhakate A R, Saha S K, Mahapatra S, Chaudhari H S, Pokhrel S and Sahu S K 2012 Why is Indian Ocean warming consistently; *Climate Change* **110** 709–719, doi: [10.1007/s10584-011-0121-x](https://doi.org/10.1007/s10584-011-0121-x).
- Ratnam J V, Giorgi F, Kaginalkar A and Cozzini S 2009 Simulation of the Indian monsoon using RegCM3-ROMS regional coupled model; *Clim. Dyn.* **33** 119–139, doi: [10.1007/s00382-008-0433-3](https://doi.org/10.1007/s00382-008-0433-3).
- Ravichandran M, Behringer D, Sivareddy S, Girishkumar M S, Chacko N and Harikumar H 2013 Evaluation of the global ocean data assimilation system at INCOIS: The Tropical Indian Ocean; *Ocean Model* **69** 123–135, doi: [10.1016/j.ocemod.2013.05.003](https://doi.org/10.1016/j.ocemod.2013.05.003).
- Romea R D and Allen J S 1983 On vertically propagating coastal Kelvin waves at low latitudes; *J. Phys. Oceanogr.* **13** 1241–1254.
- Saji N H, Goswami B N, Vinayachandran P N and Yamagata T 1999 A dipole mode in the tropical Indian Ocean; *Nature* **401** 360–363.
- Sanilkumar K V, Kuruvilla T V, Jogendranath D and Rao R R 1997 Observations of the Western Boundary Current of the Bay of Bengal from a hydrographic survey during March 1993; *Deep-Sea Res. (Part I)* **44** 135–145, doi: [10.1016/S0967-0637\(96\)00036-2](https://doi.org/10.1016/S0967-0637(96)00036-2).
- Sanilkumar V, Kumar K A and Pednekar P 2008 Observation on oceanographic parameters of nearshore waters off Yanam, during the cyclonic storm; *Curr. Sci.* **94** 530–536.
- Sarma M S S and Rao L G 1986 Currents and temperature structure off Godavari (east coast of India) during September 1980; *Indian J. Mar. Sci.* **15** 88–91.

- Sarma M S S and Rao L G 1989 Spectra of currents and temperature off Godavari (east coast of India); *Mahasagar* **22** 29–36.
- Schott F A and McCreary J P 2001 The monsoon circulation of the Indian Ocean; *Prog. Oceanogr.* **51** 1–120.
- Schott F, Reppin J and Fischer J 1994 Currents and transports of the monsoon current south of Sri Lanka; *J. Geophys. Res.* **99** 25,127–25,141.
- Schott F A, Xie S P and McCreary J P 2009 Indian Ocean circulation and climate variability; *Rev. Geophys.* **47**, doi: [10.1029/2007RG000245](https://doi.org/10.1029/2007RG000245).
- Shankar D 1998 *Low-frequency variability of sea level along the coast of India*; Ph.D. thesis, Goa Univ., India.
- Shankar D 2000 Seasonal cycle of sea level and currents along the coast of India; *Curr. Sci.* **78** 279–288.
- Shankar D and Shetye S R 1997 On the dynamics of the Lakshadweep high and low in southeastern Arabian Sea; *J. Geophys. Res.* **102** 12,551–12,562.
- Shankar D and Shetye S R 1999 Are interdecadal sea level changes along the Indian coast influenced by variability of monsoon rainfall? *J. Geophys. Res.* **104** 26,031–26,042.
- Shankar D and Shetye S R 2001 Why is mean sea level along the coast of India higher in the Bay of Bengal than in the Arabian Sea; *Geophys. Res. Lett.* **28** 563–565, doi: [10.1029/2000GL012,001](https://doi.org/10.1029/2000GL012,001).
- Shankar D, McCreary J P, Han W and Shetye S R 1996 Dynamics of the East India Coastal Current 1. Analytic solutions forced by interior Ekman pumping and local alongshore winds; *J. Geophys. Res.* **101** 13,975–13,991.
- Shankar D, Vinayachandran P N and Unnikrishnan A S 2002 The monsoon currents in the north Indian Ocean; *Prog. Oceanogr.* **52** 63–120.
- Shankar D, Aparna S G, McCreary J P, Suresh I, Neetu S, Durand F, Shenoi S S C and Saafani M A A 2010 Minima of interannual sea-level variability in the Indian Ocean; *Prog. Oceanogr.* **84** 225–241.
- Shcherbinin A D, Arsenyev V S and Yu A 1979 The western boundary current of the Bay of Bengal; *Dokl. Acad. Sci. USSR, Earth Sci. Sect.* **244** 167–168.
- Shenoi S S C, Saji P K and Almeida A M 1999 Near-surface circulation and kinetic energy in the tropical Indian Ocean derived from Lagrangian drifters; *J. Mar. Res.* **57** 885–907.
- Shenoi S S C, Shankar D and Shetye S R 2002 Differences in heat budgets of the near-surface Arabian Sea and Bay of Bengal: Implications for the summer monsoon; *J. Geophys. Res.* **107**; doi: [10.1029/2000JC000679](https://doi.org/10.1029/2000JC000679).
- Shetye S R and Shenoi S S C 1988 Seasonal cycle of surface circulation in the coastal North Indian Ocean; *Proc. Indian Acad. Sci. (Earth Planet. Sci.)* **97** 53–62.
- Shetye S R and Gouveia A D 1998 Coastal circulation in the North Indian Ocean: Coastal segment (14, S-W); *The Sea* **11** 523–556.
- Shetye S R, Gouveia A D, Shenoi S S C, Sundar D, Michael G S, Almeida A M and Santanam K 1990 Hydrography and circulation off the west coast of India during the southwest monsoon 1987; *J. Mar. Res.* **48** 359–378.
- Shetye S R, Gouveia A D, Shenoi S S C, Michael G S, Sundar D, Almeida A M and Santanam K 1991a The coastal current off western India during the northeast monsoon; *Deep-Sea Res. (Part I)* **38** 1517–1529.
- Shetye S R, Shenoi S S C, Gouveia A D, Michael G S, Sundar D and Nampoothiri G 1991b Wind-driven coastal upwelling along the western boundary of Bay of Bengal during southwest monsoon; *Cont. Shelf. Res.* **11** 1397–1408.
- Shetye S R, Gouveia A D, Shenoi S S C, Sundar D, Michael G S and Nampoothiri G 1993 The western boundary current of the seasonal subtropical gyre in the Bay of Bengal; *J. Geophys. Res.* **98** 945–954.
- Shetye S R, Gouveia A D, Shankar D, Shenoi S S C, Vinayachandran P N, Sundar D, Michael G S and Nampoothiri G 1996 Hydrography and circulation in the western Bay of Bengal during the northeast monsoon; *J. Geophys. Res.* **101** 14,011–14,025.
- Sikhakolli R, Sharma R, Basu S, Gohil B S, Sarkar A and Prasad K V S R 2013 Evaluation of OSCAR ocean surface current product in the tropical Indian Ocean using *in-situ* data; *J. Earth Syst. Sci.* **122** 187–199.
- Somayaajulu Y, Murthy V and Sarma Y 2003 Seasonal and inter-annual variability of surface circulation in the Bay of Bengal from TOPEX/Poseidon altimetry; *Deep-Sea Res. (Part II)* **50** 867–880.
- Sprintall J and Tomczak M 1992 Evidence of barrier layer in the surface layer of the tropics; *J. Geophys. Res.* **97** 7305–7316.
- Sreenivas P, Gnanaseelan C and Prasad K V S R 2012 Influence of El Niño and Indian Ocean Dipole on sea level variability in the Bay of Bengal; *Global Planet. Change* **80–81** 215–225, doi: [10.1016/j.gloplacha.2011.11.001](https://doi.org/10.1016/j.gloplacha.2011.11.001).
- Srinivas K, Kumar P K D and Revichandran C 2005 ENSO signature in the sea level along the coastline of the Indian subcontinent; *Indian J. Mar. Sci.* **34** 225–236.
- Stammer D, Wunsch C, Fukumori I and Marshall J 2002a State estimation in modern oceanographic research; *EOS Trans. AGU* **83(289)** 294–295.
- Stammer D, Wunsch C, Giering R, Eckert C, Heimbach P, Marotzke J, Adcroft A, Hill C N and Marshall J 2002b The global ocean circulation during 1992–1997, estimated from ocean observations and a general circulation model; *J. Geophys. Res.* **107** 3118, doi: [10.1029/2001JC000888](https://doi.org/10.1029/2001JC000888).
- Stommel H 1948 The westward intensification of wind-driven ocean currents; *Trans. AGU* **29(2)** 202–206.
- Sverdrup H U 1947 Wind-driven currents in a baroclinic ocean with application to the equatorial currents of the eastern Pacific; *Proceedings of the National Academy of Sciences* **33(11)** 318–326.
- Varkey M J, Murty V S N and Suryanarayana A 1996 Physical oceanography of the Bay of Bengal and Andaman Sea; *Oceanogr. Mar. Biol.* **34** 1–70.
- Vialard J, Shenoi S S C, McCreary J P, Shankar D, Durand F, Fernando V and Shetye S R 2009 Intraseasonal response of the northern Indian Ocean coastal waveguide to the Madden-Julian Oscillation; *Geophys. Res. Lett.* **36** L14606, doi: [10.1029/2009GL038,450](https://doi.org/10.1029/2009GL038,450).
- Vinayachandran P N and Kurian J 2007 Hydrographic observations and model simulation of the Bay of Bengal freshwater plume; *Deep-Sea Res. (Part I)* **54** 471–486.
- Vinayachandran P N and Yamagata T 1998 Monsoon response of the sea around Sri Lanka: Generation of thermal domes and anticyclonic vortices; *J. Phys. Oceanogr.* **28** 1946–1960.
- Vinayachandran P N, Shetye S R, Sengupta D and Gadgil S 1996 Forcing mechanisms of the Bay of Bengal circulation; *Curr. Sci.* **71** 753–763.
- Vinayachandran P N, Masumoto Y, Mikawa T and Yamagata T 1999 Intrusion of southwest monsoon current into the Bay of Bengal; *J. Geophys. Res.* **104** 11077–11085.
- Vinayachandran P N, Murty V S N and Babu V R 2002 Observations of barrier layer formation in the Bay of Bengal during summer monsoon; *J. Geophys. Res.* **107** C128018, doi: [10.1029/2001JC000831](https://doi.org/10.1029/2001JC000831).
- Vinayachandran P N, McCreary J P, Hood R R and Kohler K E 2005 A numerical investigation of the phytoplankton

- bloom in the Bay of Bengal during northeast monsoon; *J. Geophys. Res.* **110** C12001, doi: [10.1029/2005JC002966](https://doi.org/10.1029/2005JC002966).
- Webster P J, Moore A M, Loschnigg J P and Leben R R 1999 Coupled ocean–atmosphere dynamics in the Indian Ocean during 1997–98; *Nature* **401** 356–360.
- Wu L, Wang F, Yuan D and Cui M 2007 Evolution of freshwater plumes and salinity fronts in the northern Bay of Bengal; *J. Geophys. Res.* **112** C08017, doi: [10.1029/2005JC003308](https://doi.org/10.1029/2005JC003308).
- Wu G, Guan Y, Liu Y, Yan J and Mao J 2012 Air–sea interaction and formation of the Asian summer monsoon onset vortex over the Bay of Bengal; *Clim. Dyn.* **38** 261–279, doi: [10.1007/s00382-010-0978-9](https://doi.org/10.1007/s00382-010-0978-9).
- Wyrtki K 1975 El Niño – the dynamic response of the equatorial Pacific Ocean to atmospheric forcing; *J. Phys. Oceanogr.* **5** 572–584.
- Yu L, O’Brien J J and Yang J 1991 On the remote forcing of the circulation in the Bay of Bengal; *J. Geophys. Res.* **96** 20,449–20,454, doi: [10.1029/91JC02424](https://doi.org/10.1029/91JC02424).

*MS received 1 November 2013; revised 7 May 2014; accepted 9 May 2014*